AGU PUBLICATIONS

JGR

Journal of Geophysical Research: Atmospheres

RESEARCH ARTICLE
10.1002/2013JD021185

Key Points:
- Satellite demonstrates springtime transport of NO_x over Korea and Japan
- Transport from China explains large NO_2 columns over the Yellow Sea
- Transport of NO_x is important in understanding local budget of NO_x

Supporting Information:
- Readme
- Figure S1
- Figure S2
- Figure S3

Correspondence to:
S.-W. Kim,
siwan.kim@noaa.gov

Citation:
Lee, H.-J., S.-W. Kim, J. Brioude, O. R. Cooper, G. J. Frost, C.-H. Kim, R. J. Park, M. Trainer, and J.-H. Woo (2014), Transport of NO_x in East Asia identified by satellite and in situ measurements and Lagrangian particle dispersion model simulations, *J. Geophys. Res. Atmos.*, *119*, doi:10.1002/2013JD021185.

Received 12 NOV 2013
Accepted 20 DEC 2013
Accepted article online 8 JAN 2014

Transport of NO_x in East Asia identified by satellite and in situ measurements and Lagrangian particle dispersion model simulations

H.-J. Lee[1,2,3], S.-W. Kim[2,3], J. Brioude[2,3], O. R. Cooper[2,3], G. J. Frost[2,3], C.-H. Kim[1], R. J. Park[4], M. Trainer[2], and J.-H. Woo[5]

[1]Department of Atmospheric Sciences, Pusan National University, Busan, South Korea, [2]Chemical Sciences Division, NOAA Earth System Research Laboratory, Boulder, Colorado, USA, [3]Cooperative Institute for Research in Environmental Sciences, University of Colorado Boulder, Boulder, Colorado, USA, [4]School of Earth and Environmental Sciences, Seoul National University, Seoul, South Korea, [5]Department of Advanced Technology Fusion, Konkuk University, Seoul, South Korea

Abstract Nitrogen dioxide (NO_2) columns observed from space have been useful in detecting the increase of nitrogen oxides (NO_x) emissions in East Asia, particularly China, coinciding with rapid economic growth during the past several decades. NO_2 columns retrieved above a particular location reflect a combination of local NO_x emissions and transported NO_x from upwind sources. In this study, we demonstrate the transport of NO_x emitted in East Asia using satellite and surface in situ measurements and Lagrangian particle dispersion model simulations. Enhanced satellite NO_2 columns in the Yellow Sea (between China and South Korea) and the East Sea (between South Korea and Japan), and different seasonal variations of NO_2 in China, North and South Korea, and Japan, suggest the importance of NO_x transport in understanding the local NO_x budget. Lagrangian transport model simulations with tracers of different chemical lifetimes identify source-receptor relationships that explain high NO_2 over the oceans and springtime peaks in Korea and Japan, with China being the most likely source region. Our results have important implications for studies using satellite NO_2 retrievals to derive NO_x emissions at local scales in regions adjacent to large sources, such as in East Asia, Europe, and the Eastern U.S.

1. Introduction

Nitrogen oxides (NO_x), defined as the sum of nitric oxide (NO) and nitrogen dioxide (NO_2), are released to the troposphere as a result of anthropogenic activity, such as fossil fuel combustion, fertilizer application, and prescribed burning, and natural phenomena like lightning, wildfires, and soil microbial activity. NO_x play an important role in tropospheric chemistry as a major precursor of ozone and aerosols, which in turn affect air quality and climate [*Lawrence and Crutzen*, 1999; *Wild et al.*, 2001; *Lamarque et al.*, 2005].

Satellite instruments have monitored NO_2 levels in the troposphere for nearly 20 years [*Bovensmann et al.*, 1999; *Burrows et al.*, 1999; *Levelt et al.*, 2006; *Valks et al.*, 2011], and these observations have played a critical role in detecting the rapid changes in emissions and atmospheric concentrations of NO_x in China resulting from economic development [*Richter et al.*, 2005; *van der A et al.*, 2006; *Zhang et al.*, 2007; *Stavrakou et al.*, 2008; *van der A et al.*, 2008; *Lin*, 2012]. Similarly, satellite measurements indicate a large decrease in U.S. NO_x emissions due to pollution controls during the past few decades [*Kim et al.*, 2006; *Stavrakou et al.*, 2008; *Kim et al.*, 2009; *Duncan et al.*, 2010; *Russell et al.*, 2012]. Long-term observations of satellite NO_2 columns can constrain NO_x emission inventories and therefore greatly reduce uncertainties in model simulations [*Martin et al.*, 2003a; *Kim et al.*, 2006, 2011; *Lamsal et al.*, 2011; *Wang et al.*, 2012].

The chemical lifetime of NO_x is primarily determined by its conversion to nitric acid (HNO_3) and organic nitrates. OH levels in the atmosphere mainly control the lifetime of NO_x in daytime and summertime, while nitrate (NO_3) chemistry involving heterogeneous processes is important during nighttime and winter [*Calvert et al.*, 1985]. The chemical lifetime of NO_x is generally recognized to be 5–10 days in the upper troposphere [*Jaeglé et al.*, 1998], while it is about 1 day in the atmospheric boundary layer [*Leue et al.*, 2001; *Granier and Brasseur*, 2003; *Jaeglé et al.*, 2004]. Because of the rapid interconversion between NO and NO_2 in the sunlit atmosphere (on the order of minutes), we refer to the transported species of interest as NO_x, even though measurements used in this work are exclusively of NO_2. In the boundary layer, the lifetime of NO_x is ~6 h in summer, ~6–12 h in spring and fall, and ~12–20 h in winter due to changes in photolysis rate and water vapor content in the atmosphere [*Martin et al*., 2003a; *Lamsal et al*., 2010]. Therefore, a satellite NO_2 column observed over a source with a steady NO_x emission rate (e.g., urban region) is expected to have its maximum in winter, a decrease from winter to summer, its minimum in summer, and an increase from summer to winter, following changes in NO_x lifetime in the boundary layer.

NO_x lifetime strongly affects the distances over which it can be transported. For example, *Stohl et al*. [2002] found that NO_x can be transported on intercontinental scales assuming a lifetime of 5–10 days, while *Wenig et al*. [2003], using both satellite data and NO_x tracers simulated by a Lagrangian particle dispersion model, found that NO_x from large power plants in South Africa can be transported to Australia. Focusing on East Asia, the impact of long-range transport of air pollutants such as carbon monoxide, sulfur dioxide, anthropogenic aerosols, and natural dust from China on neighboring countries has been examined [*Carmichael et al*., 2002; *Park et al*., 2005; *Lin et al*., 2005; *Uno et al*., 2009]. Other studies have shown that ozone and ozone precursors emitted from China are transported across the North Pacific Ocean, which affects surface ozone in the U.S. through chemical transformations that occur during transport [*Liu et al*., 2003; *Liang et al*., 2004; *Zhang et al*., 2008; *Lin et al*., 2012]. Given the rapid and continuing increase in ozone precursor emissions in East Asia [*Richter et al*., 2005; *Hilboll et al*., 2013], an up-to-date assessment of the distribution and transport of NO_x across the region is necessary to assess the current impact of local and upwind sources of NO_x on regional air quality.

The goal of this study is to identify current sources and transport pathways of NO_x within East Asia, focusing on China, South Korea, and Japan, using satellite tropospheric NO_2 column retrievals and surface in situ data. We use the FLEXPART Lagrangian particle dispersion model [*Stohl et al*., 2005] to quantify the impact of China on NO_2 columns above neighboring countries. A new result from this analysis is the conclusion that NO_x emissions from China increase tropospheric column NO_2 above North and South Korea, which indicates that satellite observations of tropospheric column NO_2 above North and South Korea cannot be used to quantify their NO_x emissions unless the impact of Chinese emissions is taken into account.

2. Methods

2.1. Satellite Measurements

We employed the Ozone Monitoring Instrument (OMI) tropospheric NO_2 data retrieved by KNMI (DOMINO product version 2.0), NASA Goddard Space Flight Center (GSFC; NASA standard product), and the University of Bremen. The OMI aboard the Aura satellite provides measurements of solar backscatter in the ultraviolet-visible range from 270 to 500 nm. Aura was launched on 14 July 2004 into a Sun-synchronous polar orbit at approximately 705 km altitude with a local equator crossing time of 13:45 in the ascending node [*Levelt et al*., 2006; *Lamsal et al*., 2010]. These three retrievals use the same modified DOAS (Differential Optical Absorption Spectroscopy) spectral analysis method to derive NO_2 slant column densities but have the differences in calculation of stratospheric column and air mass factor (AMF). The slant columns of NO_2 are obtained from the OMI reflectance spectra in the 405–465 nm window using the DOAS technique [*Platt and Stutz*, 2008] in three retrieval algorithms: the slant column represents the integrated abundance of NO_2 along the average photon path from the sun through the atmosphere to the satellite. The tropospheric slant column is obtained by subtracting stratospheric column from total slant column. Then, the tropospheric slant column is converted to a vertical column with the tropospheric AMF, defined as the ratio of slant column density of the absorber along the slant optical path to the vertical column density [*Eskes and Boersma*, 2003; *Dirksen et al*., 2011].

In DOMINO algorithm [*Boersma et al*., 2007, 2011], the stratospheric and tropospheric contributions to the OMI NO_2 slant columns are derived by assimilating the slant columns of a global chemistry and transport model, TM4 [*Dentener et al*., 2003; *Boersma et al*., 2007, 2011]. The altitude-dependent AMFs are calculated with the Doubling Adding KNMI radiative transfer model [*Stammes*, 2001] version 3.0, using the cloud parameters based on the cloud model of *Acarreta et al*. [2004] and surface reflectivity from the OMI surface albedo climatology [*Kleipool et al*., 2008].

For NASA standard product (see http://disc.sci.gsfc.nasa.gov/Aura/data-holdings/OMI/documents/v003/OMNO2_readme_v003.pdf for more detail), estimating for stratosphere-troposphere separation requires a monthly tropospheric climatology, but this is applied only to areas with relatively little tropospheric NO_2 such as clean regions or areas cloudy enough to effectively block the satellite's view of tropospheric NO_2. In substantially polluted conditions, the stratosphere is estimated by spatial interpolation from the surrounding clean regions [*Bucsela et al.*, 2013]. The monthly mean NO_2 profile shapes derived from GSFC Global Modeling Initiative chemical transport model multiannual (2005–2007) simulations are used in the AMF calculations. NASA OMI product uses the same cloud fraction and surface albedo as the DOMINO product.

The University of Bremen OMI data use the reference sector method to separate stratospheric and tropospheric columns. Model for OZone And Related chemical Tracers (MOZART) model NO_2 profile and Low Resolution Atmospheric Radiance and Transmittance Model (LOWTRAN) aerosol assumptions are used to determine AMFs [*Kim et al.*, 2009].

KNMI tropospheric NO_2 retrieval (http://www.temis.nl/airpollution/no2.html) from SCanning Imaging Absorption spectroMeter for Atmospheric CHartographY (SCIAMACHY) [*Bovensmann et al.*, 1999] and the Second Global Ozone Monitoring Experiment (GOME2) [*Valks et al.*, 2011] were also utilized to derive the trends over East Asia.

2.2. Surface In Situ Measurement Data

Rural and urban surface NO_2 mixing ratios in South Korea are assessed for 2005–2009 using in situ NO_2 observations collected hourly by the surface monitoring system operated by the Korea Ministry of Environment, which presently includes over 300 stations. Chemiluminescence with a molybdenum catalytic converter was used to measure NO_2 at all sites. Previous studies [e.g., *Fehsenfeld et al.*, 1987; *Dunlea et al.*, 2007; *Lamsal et al.*, 2010] indicate that this method measures not only NO_2 but also other reactive nitrogen species. To minimize the interference of other reactive nitrogen species, we use the NO_2 data measured in the early morning at 07:00–09:00 Local Standard Time (LST) instead of the data measured at the OMI overpass time. The results using the NO_2 data observed between 12:00 and 15:00 LST (close to the OMI overpass time, 13:45 LST) are shown in the supporting information Figure S1; they are qualitatively similar to the results using the observations in the early morning. Since the satellite retrieval algorithm rejects the data when the cloud fraction is more than 30%, we also filtered out the surface NO_2 measurements when the cloud cover was more than 30%, according to cloudiness data measured every 3 h at the Korea Meteorological Administration meteorological observation station nearest to the NO_2 measurement site. Monthly averages of NO_2 mixing ratios for five urban areas and three rural or remote sites were calculated and are used to evaluate the signals in the monthly averaged satellite data. The urban areas examined (number of stations used) are Seoul (27), Busan (13), Daegu (7), Gwangju (4), and Gwangyang (2), and the rural/remote areas examined (number of stations used) are Taean (1), Ulleungdo (1), and Gosan (1). O_3 mixing ratios measured at the surface sites were also used for trend analysis.

2.3. Lagrangian Particle Dispersion Model

The Lagrangian particle dispersion model, FLEXPART version 8.0 [*Stohl et al.*, 2005], is used to identify the source and receptor regions of NO_x in East Asia. This model was designed to simulate the long-range and regional-scale dispersion of air pollutants and has been used to understand transport of anthropogenic, biomass burning, and volcanic emissions [*Stohl et al.*, 2007; *Brioude et al.*, 2009; *Warneke et al.*, 2009; *Stohl et al.*, 2011]. FLEXPART was driven by National Centers for Environmental Prediction Global Forecast System wind fields with a temporal resolution of 3 h (analyses at 00, 06, 12, 18UTC and 3 h forecasts at 03, 09, 15, 21UTC), horizontal resolution of $0.5° \times 0.5°$, and 27 vertical levels. The horizontal resolution of the FLEXPART output domain was $0.25° \times 0.25°$, with 25 vertical levels between 0 and 30 km (the first layer from 0 to 0.1 km, 23 layers with vertical resolution of 500 m from 0.5 km to 12 km, and the top layer from 12 km to 30 km).

FLEXPART was run for 2010 with a passive anthropogenic NO_x tracer with lifetimes ranging from 6 h to 48 h. About 276 area sources of NO_x at $2° \times 2°$ resolution over East Asia (China, Korea, and Japan (Figure 1)) were designated to investigate the NO_x source-receptor relationships in detail. Simulations were carried out including emissions from either all sources or just the sources in a specific area (China, Korea, or Japan).

10.1002/2013JD021185

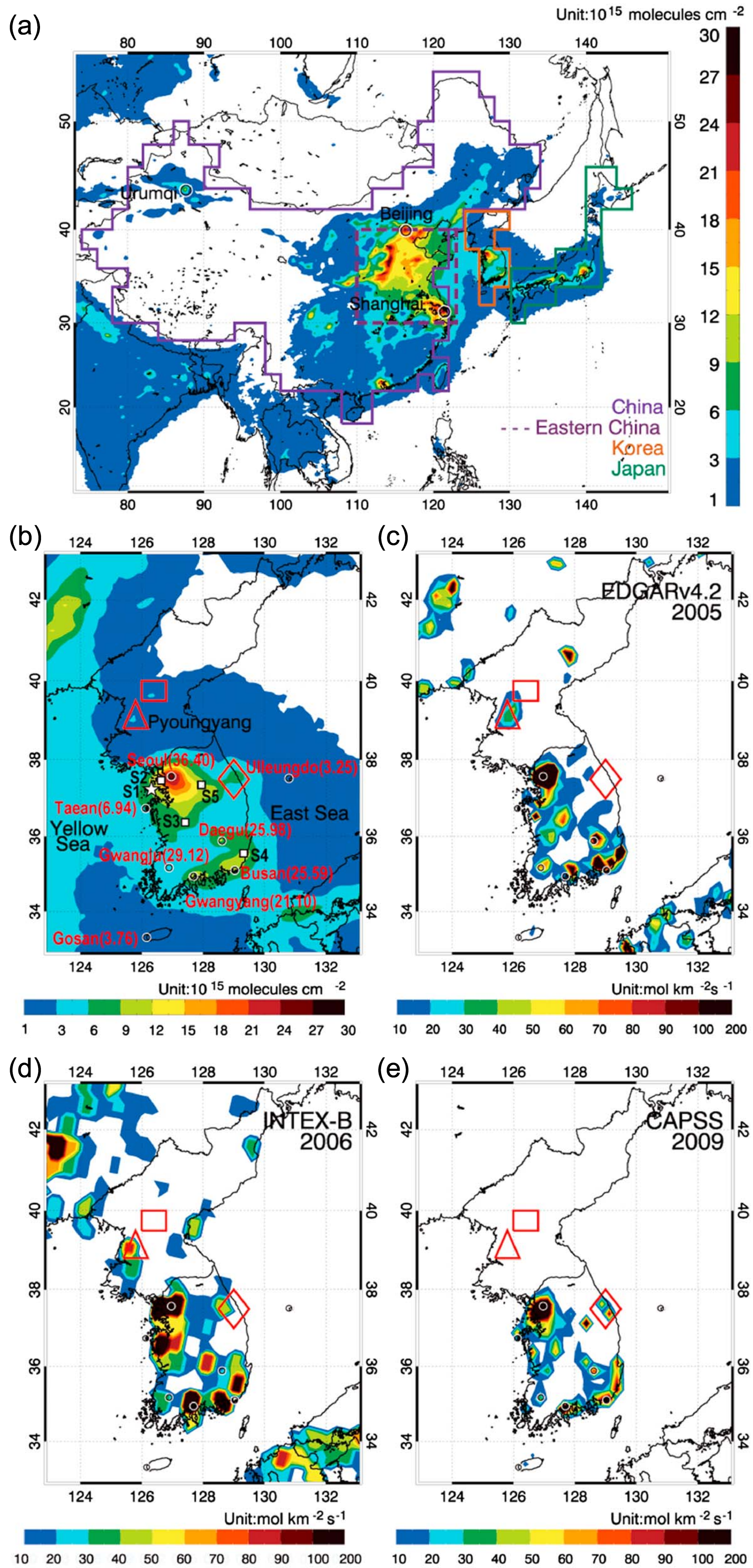

Figure 1

2.4. Emissions Inventories

The anthropogenic NO_x emissions used by FLEXPART were derived from two inventories: (1) the 2006 Intercontinental Chemical Transport Experiment-Phase B (INTEX-B) Asia emission data set [*Zhang et al.*, 2009] with spatial resolution of 0.5° × 0.5°, and (2) the Emission Database for Global Atmospheric Research (EDGAR) v4.2 for base year 2005, spatially allocated on a 0.1° × 0.1° grid.

In addition to INTEX-B and EDGAR, the CAPSS09 (Clean Air Policy Support System; http://airemiss.nier.go.kr) inventory was used in the satellite analysis. CAPSS09 is the product of the Korean national emission inventory system for the year 2009, which estimates seven criteria air pollutants used in national air quality modeling (i.e. SO_2, NO_x, NMVOC, CO, PM10, PM2.5, and NH_3). In CAPSS, 982 emissions sources categories and 145 fuel types are classified into four different sector levels. The native spatial resolution of the inventory is the 251 second-level administrative units (i.e. counties). All activity data in CAPSS are submitted from 150 domestic organizations in Korea, while it incorporates emission factors from domestic and international research reports.

3. Results

3.1. Spatial Distribution of NO_2 Columns

Figure 1 shows the spatial distributions of OMI tropospheric NO_2 column in East Asia and in North and South Korea, in particular, during 2005–2011. Enhanced tropospheric NO_2 columns occurred over megacities and industrial regions, such as central eastern China, Hong Kong, much of South Korea, and central and western Japan. The regions of high NO_2 spread across eastern and central China, ranging from south of the Yangtze Delta region near Shanghai (121°28′E, 31°13′N) to north of Beijing (116°24′E, 39°54′E). A few isolated enhancements are seen over Urumqi, a medium-sized city in the western part of China where there are some large NO_x point sources (Figure 1) [see *van der A et al.*, 2006]. It is noteworthy that NO_2 columns reach up to 6×10^{15} molecules cm^{-2} over the Yellow Sea between China and Korea, and similar levels are seen over the East Sea between Korea and Japan. These NO_2 columns are comparable to those observed above two of the largest power plants in the U.S. (e.g., Four Corners and San Juan power plants; see *Kim et al.* [2009] for details). In Japan high tropospheric NO_2 columns occurred above Tokyo and the southwestern urban and industrial regions (Kyoto, Nagoya, Kobe, and Hiroshima).

Detailed images of OMI NO_2 columns and the bottom-up NOx emissions from EDGARv4.2, INTEX-B, and CAPSS09 over Korea are also shown in Figure 1, along with average NO_2 mixing ratios measured at surface monitors in South Korea. In South Korea, relatively high OMI NO_2 columns are seen over two large cities, Seoul and Busan, and a large industrial region, Gwangyang. In situ measurements also exhibit high annual average mixing ratios of NO_2 in Seoul (36.40 ppbv), Busan (25.59 ppbv), Gwangju (29.12 ppbv), Gwangyang (21.10 ppbv), and Daegu (25.98 ppbv). The urban areas in South Korea identified by the bottom-up emissions inventory correspond to regions with higher NO_x levels detected by the satellite and in situ surface measurements. The annual average NO_2 surface mixing ratios at Gwangju (29.12 ppbv) are probably high relative to the satellite retrievals ($3–6 \times 10^{15}$ molecules cm^{-2}) due to the close proximity of the urban surface NO_2 monitors to automobile and tire factories.

OMI also indicates two Korean source regions that are absent in the EDGAR inventory. A strong isolated source in the OMI data is located in the Donghae-Samchock area in northeastern South Korea near the East Sea (Figure 1, diamond symbol). This area is well known for large cement industrial facilities and also has medium-sized coal-burning power plants. Two isolated and relatively weak sources are seen in North Korea: Pyongyang (capital city of North Korea, triangle symbol) and Sunchŏn (site of several large power plants and industrial facilities, rectangular symbol). The emission inventory (EDGARv4.2) does not include

Figure 1. Spatial distribution of (a) OMI tropospheric NO_2 columns averaged over 2005–2011 for East Asia, (b) OMI tropospheric NO_2 columns averaged over 2005–2011 for North and South Korea, (c) EDGARv4.2 NO_x emissions, (d) INTEX-B NO_x emissions, and (e) CAPSS09 NO_x emissions over South Korea. Boundaries marked by purple, orange, and green solid lines in Figure 1a encompass the regions of China, Korea, and Japan, respectively, that are used for calculating statistics. The dotted purple line in Figure 1a denotes Eastern China (also used in *Richter et al.* [2005]). Rectangular boxes, triangles, and diamonds in Figures 1b–1e represent industrial and capital areas (Pyongyang) in North Korea and industrial and power plant regions in Donghae, South Korea, respectively. Annual averages of in situ NO_2 mixing ratios (ppbv) at various locations in South Korea are included in Figure 1b. The white star in Figure 1b indicates the surface monitoring site at Deokjeokdo (S1) analyzed in Figure 5. The white squares in Figure 1b show the locations of Wonju (S2), Daejeon (S3), Ulsan (S4), and Wonju (S5) used in Figures 13 and 14.

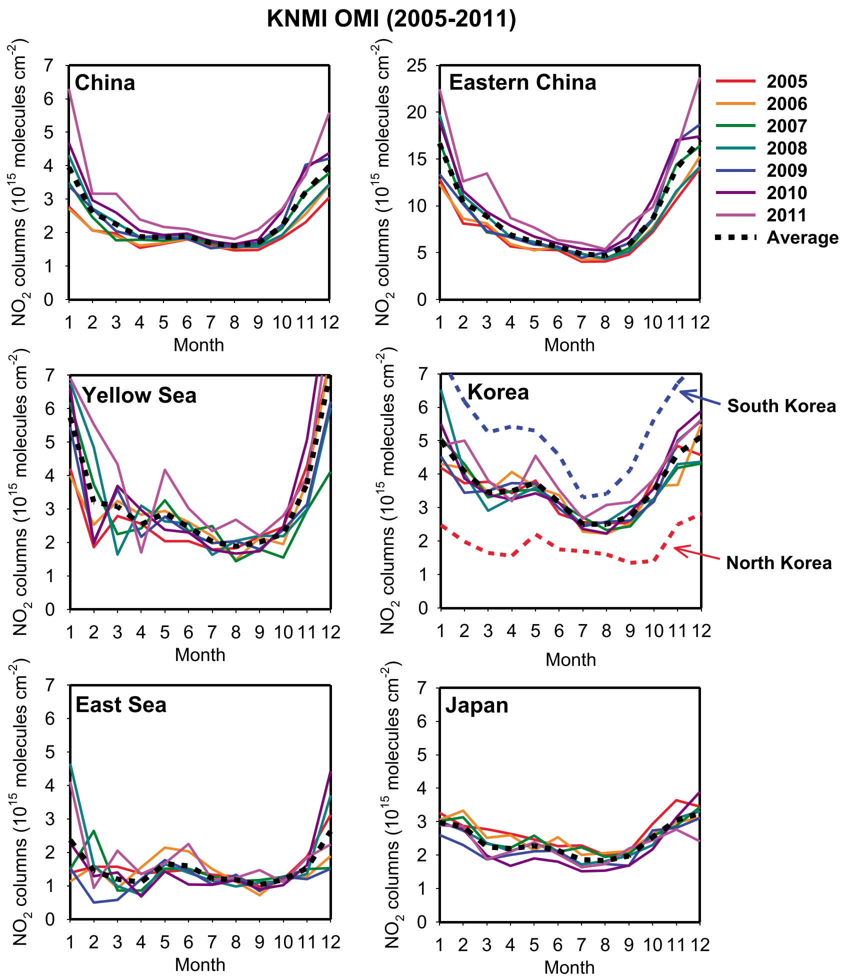

Figure 2. Monthly variations in NO_2 columns from the OMI satellite instrument over China, Eastern China, Yellow Sea, Korea, East Sea, and Japan for each year in the period 2005–2011. Dashed black lines denote averages of the data from 2005 to 2011. Blue and red dashed lines represent averages over South and North Korea, respectively.

any large industrial sources and power plants in the Donghae-Samchock area and the Sunchŏn area, where the satellite data show enhanced NO_2 columns. The INTEX-B and CAPSS09 inventories have large emissions over the Donghae-Samchock area in northeastern South Korea, with locations of sources in the INTEX-B slightly shifted due to its coarse resolution (0.5°×0.5°). CAPSS09 is consistent with the OMI NO_2 columns over the Donghae-Samchock area in terms of spatial co-location of the emissions and the satellite-observed plumes. These comparisons illustrate that bottom-up emission inventories do not necessarily have consistent representations for North or South Korea and that the satellite observations may provide valuable information about missing sources in these inventories.

High levels of NO_2 are seen over the Yellow Sea and the East Sea, where according to EDGAR v4.2, ship NO_x emissions over the Yellow Sea and the East Sea are 0.66% and 0.37% of the emissions from all of China, respectively. The NO_2 detected here may be mainly due to transport of NO_x emitted from land-based sources, rather than direct emissions from marine areas.

3.2. Seasonal Variations of Satellite NO_2 Columns and Surface Observations

To investigate the regional seasonal variations of NO_2 columns, we subdivided East Asia into four regions: China, Eastern China, Korea, and Japan (see Figure 1 for the definitions). In addition, two marine regions between the countries are also defined: the Yellow Sea (123°E ≤ longitude < 126°E, 32°N ≤ latitude < 38°N) and the East Sea (130°E ≤ longitude < 133°E, 36°N ≤ latitude < 40°N). Figure 2 presents the monthly variations

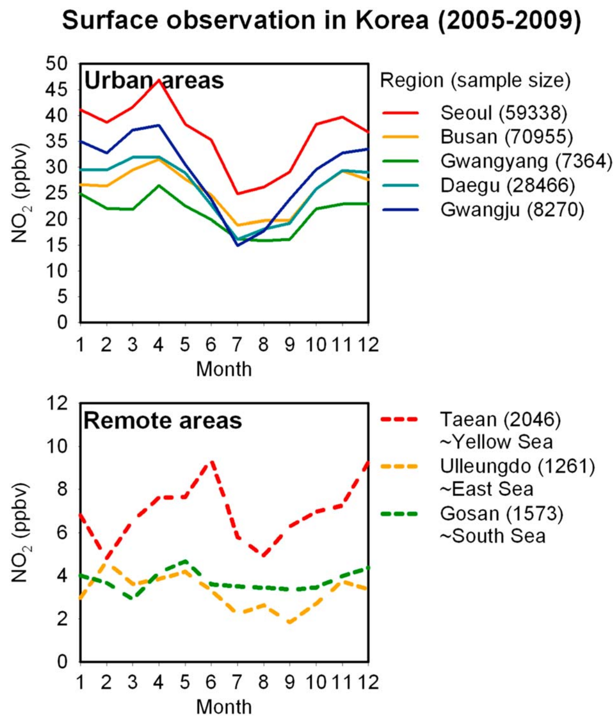

Figure 3. Monthly variations in average surface NO_2 mixing ratio observations at 0700–0900 LST in the South Korean urban and remote sites in Seoul, Busan, Gwangyang, Daegu, Gwangju, Taean, Ulleungdo, and Gosan during 2005–2009. The number of data points used to construct each curve is enclosed in parentheses next to the name of each site in the figure legend. The locations of these sites are shown in Figure 1.

of tropospheric NO_2 columns observed from the OMI satellite instrument in these designated regions. The monthly change in China and Eastern China is characterized by a winter maximum and a summer minimum, consistent with expected seasonal variations in NO_x lifetimes. The seasonal cycle in China as a whole is less pronounced (flat from April to September) than that in Eastern China, because the larger Chinese region includes remote areas in which soil microbial activity increases NO_2 during summertime [*van der A et al.*, 2006]. Anthropogenic NO_x emissions from China do not vary significantly with season [*Zhang et al.*, 2007].

The seasonal behavior of the OMI NO_2 columns over other parts of East Asia is different from that over China. In addition to the expected seasonal variations due to NO_x lifetime, secondary peaks in NO_2 columns are seen consistently from 2005 to 2011 in the spring and early summer (March–June) over the Yellow Sea, Korea, the East Sea, and Japan. The spring peaks are clearly seen in both South Korea and relatively clean North Korea (Figure 2). The NO_2 column average over North Korea in May is comparable to that measured in the wintertime. Enhancement of NO_2 columns over North Korea during much of the summer may be caused by transport and/or soil microbial activity. Tropospheric NO_2 columns retrieved by other satellite instruments (SCIAMACHY and GOME2) also exhibit these secondary peaks (not shown).

The surface observations of NO_2 mixing ratios in South Korea show spring peaks similar to the satellite measurements. Figure 3 illustrates that in situ NO_2 mixing ratios have a major peak in wintertime and a secondary peak in springtime over large cities in South Korea as well as at remote and rural Korean sites (Figure 3). This springtime NO_2 enhancement is in agreement with the maximum in carbon monoxide (CO) seen at remote Pacific sites during this season according to previous studies [*Liu et al.*, 2003; *Liang et al.*, 2004; *Lin et al.*, 2010]. The lifetime of CO ranges from 30 days (in summer) to 60 days (in winter) at 30°–40°N [*Liang et al.*, 2004], allowing CO to be transported long distances from Asian source regions. The springtime peaks of both species suggest that NO_x can be transported similarly to CO to some extent, although the lifetime of NO_x is much shorter than that of CO.

3.3. NO_x Transport Episodes in Springtime

Figure 4 demonstrates some major episodes of NO_x transport during March–April 2010 using OMI tropospheric NO_2 columns and the FLEXPART simulation results incorporating Chinese emissions sources only. The OMI retrieval

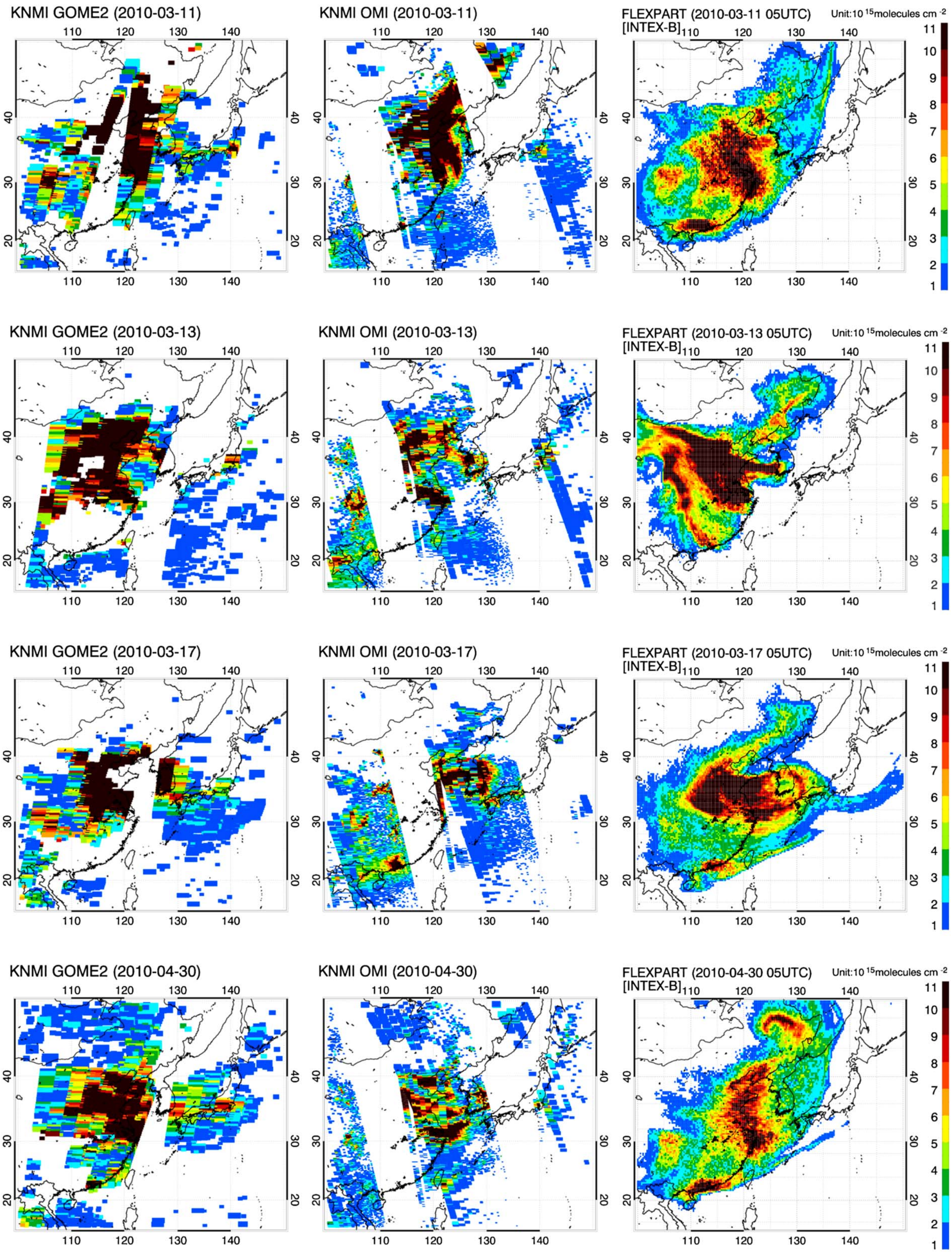

Figure 4. Major NO_x transport events in March–April 2010 as seen from tropospheric NO_2 columns retrieved from (left) GOME2 and (middle) OMI. Also shown are (right) the NO_2 columns simulated by the FLEXPART model with only Chinese emissions in INTEX-B assuming 12 h of NO_x lifetime.

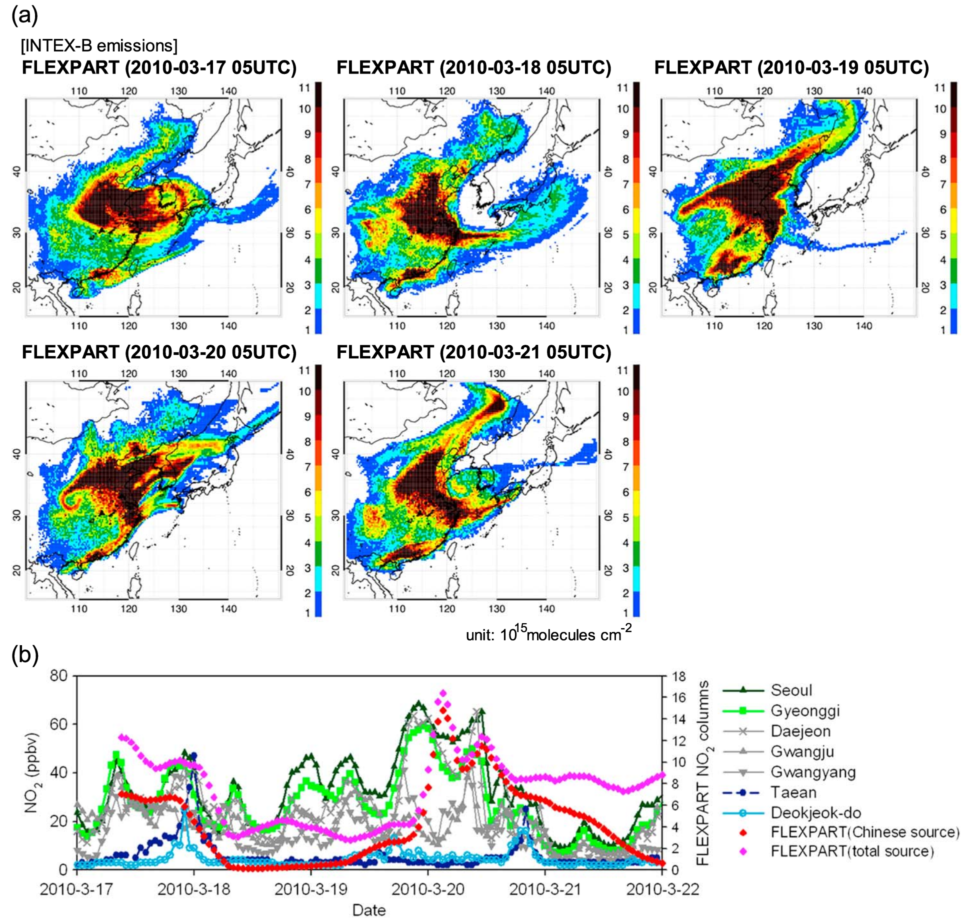

Figure 5. (a) The day-to-day variations in the spatial patterns of the FLEXPART simulated NO_2 columns during 17–21 March 2010. (b) Time series of observed hourly NO_2 mixing ratios at Taean (dark blue dashed line), Deokjeokdo (blue solid line), and several urban sites in the western part of South Korea (see Figure 1 for locations). Here Gyeonggi represents metropolitan areas of 36°N–38°N and 126°E–127°E, but it excludes Seoul. Also shown are the hourly FLEXPART NO_2 columns based on emissions from all sources in East Asia (pink) and with only Chinese emissions (red).

has many missing pixels affected by a row anomaly. In addition, clouds hinder the satellite from providing good spatial coverage over the region. Nonetheless, the FLEXPART results agree well with the spatial distributions of the GOME2 and OMI retrievals, although there are spatial shifts in the locations of the observed and simulated plumes due to the coarse definitions of the source regions (2° × 2°). Transport of Chinese emissions over the Yellow Sea, Korea, and the East Sea is evident in each of these data sets on 11 March, 13 March, 17 March, and 30 April.

The episode beginning on 17 March is examined in more detail using the FLEXPART results and surface monitor observations. Figure 5 shows spatial distributions of the FLEXPART NO_2 columns from 17 to 21 March. Large-scale transport of Chinese emissions to South Korea is simulated on 17 and 20 March, resulting from two midlatitude cyclones that traversed the Yellow Sea and Korea. The second storm also transported dust to Korea on 20 March. After the passage of each cyclone, the NO_x plumes were pushed back toward China due to the presence of surface anticyclones located above Korea, Japan, and the North Pacific Ocean. The time series of NO_2 measured at surface monitors in several areas of western South Korea (including coastal areas such as Deokjeok-do and Taean) during the 17–21 March episode are also shown in Figure 5. High mixing ratios at Deokjeok-do and Taean (up to 40 ppbv) were observed on 17 and 20 March. Strong plumes with high mixing ratios (> 60 ppbv) in the Seoul and Gyeonggi regions in the early morning (00–06 LST) were detected in the observations and were co-located concurrently with the FLEXPART Chinese plumes.

These results demonstrate that large-scale pollution monitoring from space and FLEXPART simulations are useful for detecting Chinese plume events impacting downwind regions. Surface monitors along the west

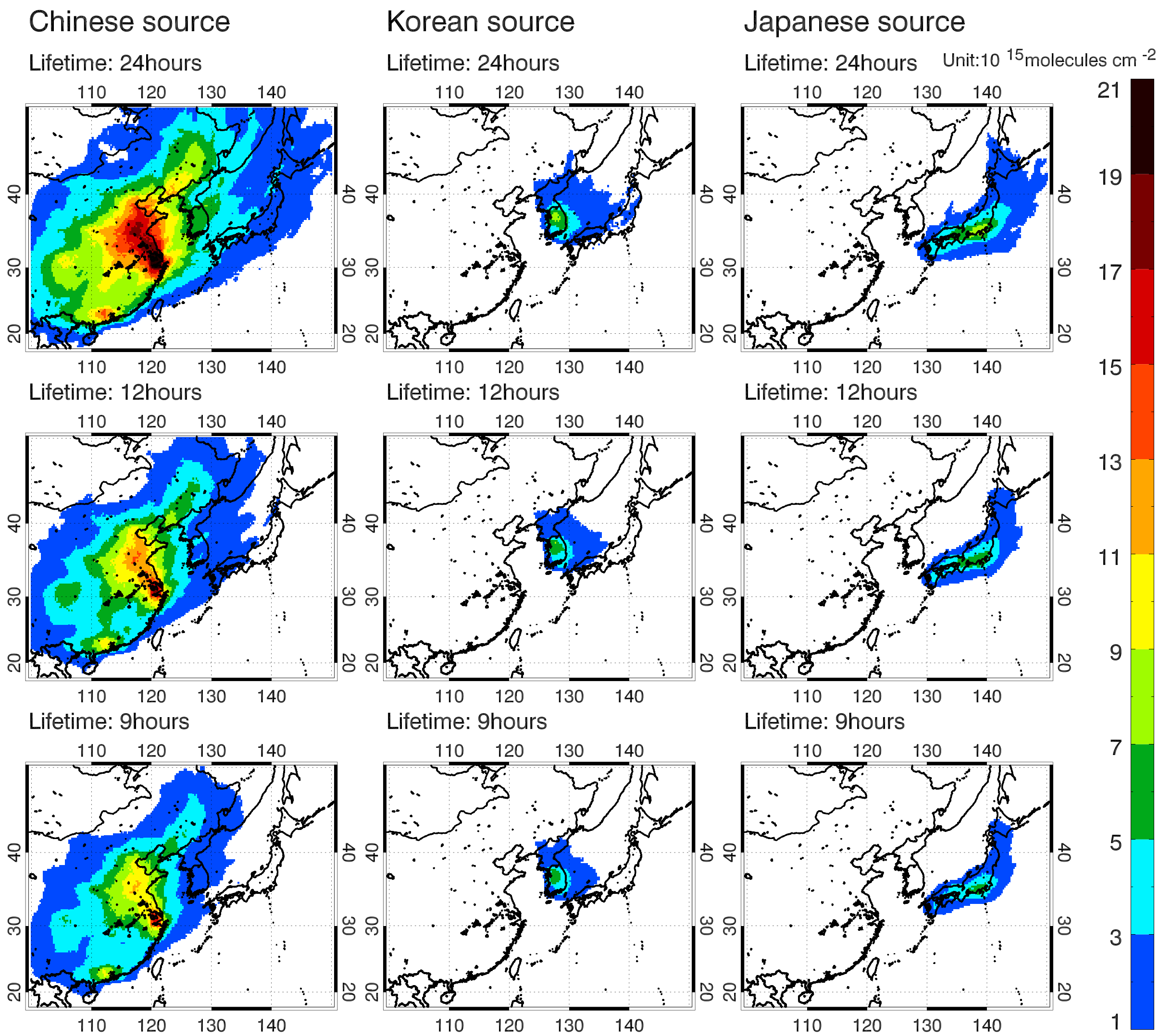

Figure 6. Spatial distributions of NO_2 columns simulated by FLEXPART for May 2010. The assumed lifetime of NO_x in the simulations changes from (top) 24 h to (bottom) 9 h. The NO_2 columns calculated using only sources in (left) China, (middle) Korea, or (right) Japan are also shown.

coast of South Korea are helpful for demonstrating the strong influence of Chinese pollution sources, especially under cloudy conditions. In the next section, we move beyond episode analysis and calculate a seasonal NO_x budget with a statistical approach using source-receptor relationships.

3.4. NO_x Budget Calculation

3.4.1. Springtime Budget Assuming Various NO_x Lifetimes

We begin with an anthropogenic NO_x budget estimate for springtime when pronounced peaks of NO_x appear in the satellite and in situ surface observations. Figure 6 presents the FLEXPART results showing the contributions of Chinese, Korean, and Japanese sources to the spatial distribution of NO_2 columns in East Asia during May 2010 with assumptions of various NO_x lifetimes (9 h to 24 h). FLEXPART indicates that the influence of NO_x emissions from China can reach the Yellow Sea, Korea, the East Sea, and Japan in springtime, while emissions from Korea can affect the East Sea and Japan. Vertical profiles of simulated NO_2 (not shown) demonstrate that transport is primarily in the lower level (< 1.5 km) and that upper level transport is less frequent or episodic. FLEXPART confirms that the relatively short lifetime of NO_x within the boundary layer (~1 day) still allows NO_x emissions to influence a large spatial domain. The FLEXPART results with NO_x lifetimes ranging from 9 to 24 h show that NO_x emissions from China can contribute 50%–70% of the total NO_2 columns above Korea in May 2010 (Table 1).

Table 1. FLEXPART Calculated Contributions (%) to NO_2 Columns From Three Source Regions: China, Korea, and Japan[a]

	Lifetime: 24 h (Averaged Column Amount)		
Receptor (Averaged Column Amount)	China (4.27)	Korea (9.15)	Japan (6.82)
Source			
China	98.30	67.09	38.22
Korea	1.33	30.65	13.52
Japan	0.37	2.26	48.26
	Lifetime: 12 h		
Receptor (Averaged Column Amount)	China (2.66)	Korea (5.58)	Japan (3.82)
Source			
China	98.86	56.77	21.79
Korea	0.99	41.58	13.25
Japan	0.15	1.65	64.96
	Lifetime: 9 h		
Receptor (Averaged Column Amount)	China (2.14)	Korea (4.39)	Japan (2.95)
Source			
China	99.07	50.94	14.83
Korea	0.84	47.71	12.34
Japan	0.09	1.35	72.83

[a]NOx lifetime of 9, 12, and 24 h were applied to the May 2010 study period. Averaged column amount unit: 10^{15} molecules cm^{-2}. Areas of China (9,659,653 km^2), Korea (391,148 km^2), and Japan (784,219 km^2) were used to calculate averaged column amount, as shown in Figure 1.

This analysis suggests the possibility that NO_x transport leads to springtime peaks in Korea and Japan. However, East Asia is known for high aerosol loading with both natural and anthropogenic origins. The role aerosols play in photochemistry in this region may also be important, according to GEOS-Chem and box model simulations [*Martin et al.*, 2003b; *Jeong and Sokolik*, 2007]. GEOS-Chem [*Park et al.*, 2004] simulations with and without the impact of aerosols on photolysis frequencies for May 2010 indicate that this impact is relatively large in China, but it is negligible in the Yellow Sea and Korea, where the difference between the cases with and without the impact of aerosols on photolysis frequency is less than 5% (see supporting information Figure S2). Studies focusing on episodes with particularly large aerosol loadings (including springtime dust storms) are needed to understand the roles of NO_x transport and chemistry-aerosol interactions under these conditions.

3.4.2. Seasonal NO_x Budgets Assuming Constant NO_x Lifetime

Figure 7 shows that the FLEXPART NO_2 columns with constant NO_x lifetimes (24 h) are dependent on the seasonal variation of transport pattern. The NO_2 columns over China, Korea, and Japan, due to each country's domestic emissions, are greatest in summer and smallest in winter, while Chinese outflow over the Yellow Sea and Korea is weakest in autumn.

The transport characteristics of synoptic systems in East Asia vary substantially from season to season [*Kim et al.*, 1997] (also see supporting information Figure S3). During winter, a continental anticyclone located over China is common, and accompanying strong northerly or northwesterly winds cause transport over longer distances with greater dilution compared to other seasons. In spring, fast eastward moving synoptic disturbances (e.g., warm conveyor belts of midlatitude cyclones or migratory anticyclones) frequently develop due to strong baroclinic instability, efficiently transporting the emissions from China to Korea and Japan. In contrast, southerly winds associated with the East Asian summer monsoon can lead to the accumulation of domestic emissions within China. When transport does occur the accumulated pollution can affect regions downwind with very strong plumes. In summer, there is also strong northeastward transport from China to regions north of North Korea. Transport of Chinese emissions over Korea is at a minimum in autumn, when a continental high-pressure system begins to develop over China with a weakened North Pacific high-pressure system east of Korea and Japan.

Source-receptor relationships assuming a constant NO_x lifetime of 24 h are summarized by season in Table 2. The Chinese contributions to NO_2 columns over Korea are greatest in winter and spring (75% and 66%, respectively) and smallest in autumn (57%). The influence of Chinese sources on Japan is greatest during winter and spring (51% and 41%, respectively) and much less in the other seasons (24%–26%). The contribution of Korean sources to Japan is about 10% in all seasons. Japanese domestic emissions explain 37%, 47%, 66%, and 64% of total Japanese NO_2 columns in winter, spring, summer, and autumn, respectively.

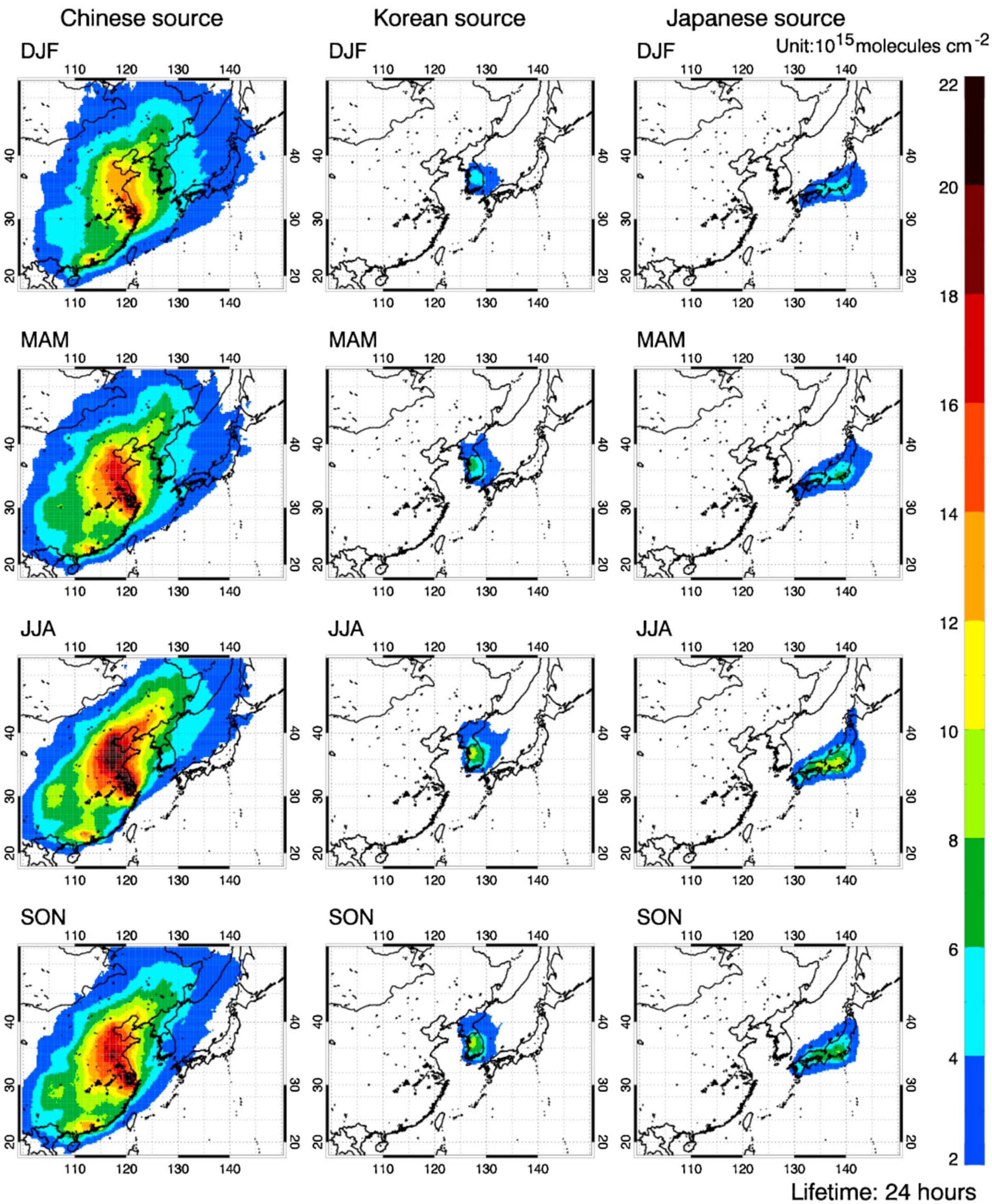

Figure 7. The FLEXPART NO_2 columns calculated using only (left) Chinese, (middle) Korean, or (right) Japanese emissions assuming a NO_x lifetime of 24 h are shown for each season (top to bottom: winter, spring, summer, and fall).

Figure 8 illustrates that Chinese emissions dominate the NO_2 columns in the Yellow Sea and North Korea throughout the year when assuming a NO_x lifetime of 24 h. The impact of Chinese emissions on North Korea is at a maximum during the summer. The influence of Chinese sources on the Yellow Sea, South Korea, and Japan is at its maximum in January/February and at its minimum in August/September/October, during

Table 2. The Seasonal Variations of FLEXPART Calculated Contributions (%) to NO_2 Columns From Three Source Regions: China, Korea, and Japan[a]

	Winter (*DJF*)		
Receptor (Average Column)	China (3.45)	Korea (9.10)	Japan (6.21)
Source			
China	97.81	75.22	50.68
Korea	1.71	23.76	12.72
Japan	0.48	1.02	36.60
	Spring (*MAM*)		
Receptor (Average Column)	China (4.29)	Korea (9.68)	Japan (6.26)
Source			
China	97.69	65.51	41.05
Korea	1.73	31.04	12.32
Japan	0.58	3.45	46.63
	Summer (*JJA*)		
Receptor (Average Column)	China (4.61)	Korea (10.86)	Japan (6.13)
Source			
China	98.81	61.98	24.27
Korea	1.04	34.92	9.48
Japan	0.15	3.10	66.25
	Autumn (*SON*)		
Receptor (Average Column)	China (4.44)	Korea (9.44)	Japan (5.43)
Source			
China	97.86	56.71	26.03
Korea	1.57	39.15	10.47
Japan	0.57	4.14	63.50

[a]A NOx lifetime of 24 h was applied to all seasons. Unit of average column: 10^{15} molecules cm^{-2}. Areas to calculate averages in parentheses are 9,659,653 km^2, 391,148 km^2, and 784,219 km^2 for China, Korea, and Japan, respectively. See Figure 1 for definitions of the areas.

which domestic emissions dominate the budget. In May, the contribution of Chinese sources to the total budget increases compared to that in March and April over the Yellow Sea, South Korea, and Japan.

The assumption of a constant NO_x lifetime of 24 h may not be reasonable, especially for summer when photochemical reaction rates are at their peak and the lifetime of NO_x is reduced relative to other seasons. In the next section we consider the impact of seasonally varying the NO_x lifetime.

3.4.3. Seasonal NO_x Budgets Assuming Seasonally Varying NO_x Lifetimes

In addition to seasonal transport patterns, seasonal changes in NO_x chemical lifetime need to be considered to calculate a realistic NO_x budget in each season. Figure 9 shows monthly mean NO_2 columns from the three OMI retrievals and the monthly FLEXPART NO_2 columns calculated with various NO_x lifetimes and two emission inventories (INTEX-B and EDGARv4.2), to provide guidance for an appropriate NO_x lifetime in each season. The FLEXPART results in summertime with 6 h lifetime and INTEX-B emissions (Figure 9, orange circles) are in good agreement with the OMI columns over all regions.

It is difficult to determine a single NO_x lifetime for winter, spring, and autumn because of large deviations among the satellite retrievals. The FLEXPART columns with a NO_x lifetime of 48 h agree best with wintertime satellite NO_2 columns over China and Eastern China. But a 48 h NO_x lifetime leads to FLEXPART NO_2 columns that are too high relative to the satellite retrievals over the Yellow Sea, North Korea, South Korea, and Japan (not shown; refer to the FLEXPART results with lifetime of 24 h over these same regions). These wintertime discrepancies may be due to errors in the emission inventory, uncertainties in the satellite retrievals, and model limitations when imposing a constant NO_x lifetime. The satellite retrievals diverge substantially above North Korea in winter, spring, and autumn, yielding a wide range of possible NO_x lifetimes, depending on the retrieval method. The model results using two different emission inventories also vary over the Yellow Sea and North Korea. Our study demonstrates the challenges in developing a quantitative NO_x budget and building an accurate source-receptor relationship for East Asia. Calibration of the satellite retrievals over East Asia is critical for the quantitative assessment of the NO_x budget and the emission inventories across this region.

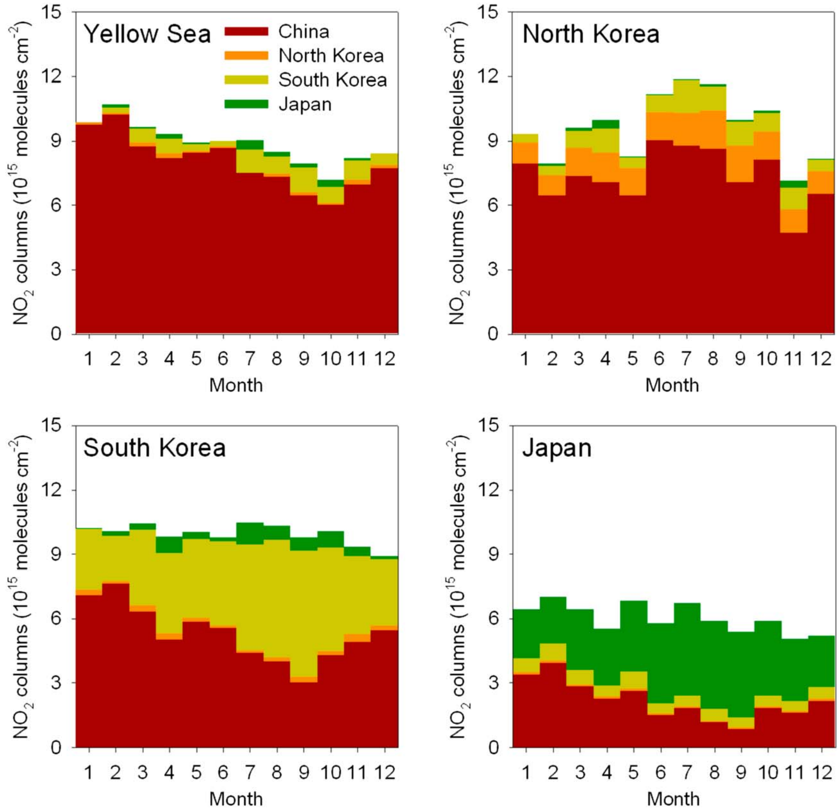

Figure 8. The monthly NO_x budget over the Yellow Sea, North Korea, South Korea, and Japan with regional source attributions calculated by FLEXPART assuming a NO_X lifetime of 24 h in winter (DJF), spring (MAM), summer (JJA), and autumn (SON).

In Table 3, the seasonal NO_x budget is estimated for NO_x lifetimes of 12, 9, 6, and 9 h in winter, spring, summer, and autumn, respectively. These particular lifetimes were chosen because the FLEXPART results agree reasonably well with the satellite retrievals over the Yellow Sea, North Korea, South Korea, and Japan. These lifetime choices are also similar to the estimates derived from previous global atmospheric chemistry model simulations [*Martin et al*., 2003a; *Lamsal et al*., 2010]. The FLEXPART results with a NO_x lifetime of 12 h in winter results in large quantities of NO_x transported from China to Korea (~70% of total NO_2 columns above Korea in Table 3). Wintertime transport may be less discernible in the satellite observations due to the fact that both the photochemical lifetime and transport lead to NO_2 maxima in this season. According to FLEXPART with a NO_x lifetime of 9 h, Chinese emissions can contribute ~50% of NO_2 columns over Korea in spring 2010, which is consistent with the springtime peaks in Korea's satellite and surface NO_2 data (see Table 3 and Figure 10). The contribution of Chinese emissions to the NO_2 columns over Korea is smaller in summer (30%) and autumn (~40%) than in winter and spring because of a significantly reduced chemical lifetime in summer and weak transport in autumn. The FLEXPART results with a NO_x lifetime of 6 h in summer indicates a relatively small, but still significant (30%), impact of transport on NO_2 columns over Korea. The contributions of Chinese and Korean emissions to the total NO_2 columns in Japan are 48%, 28%, 6%, and 15% in winter, spring, summer, and autumn, respectively (the contributions of just Korean sources are 14%, 11%, 4%, and 7%, respectively). Transported Chinese and Korean NO_x may therefore contribute to the springtime peaks of NO_2 seen in Japan. Finally, FLEXPART indicates that the contributions of NO_x transported from Korea and Japan to total NO_2 columns in China is negligible throughout all seasons (Table 3).

Figure 10 is the same as Figure 8, except that the FLEXPART simulations in Figure 10 use seasonally varying NO_x lifetimes adjusted to match the satellite observations, as described above and shown in Table 3. Figure 10 illustrates that Chinese emissions dominate the NO_2 columns over the Yellow Sea throughout the year and over North Korea in winter, spring, and autumn, which is largely consistent

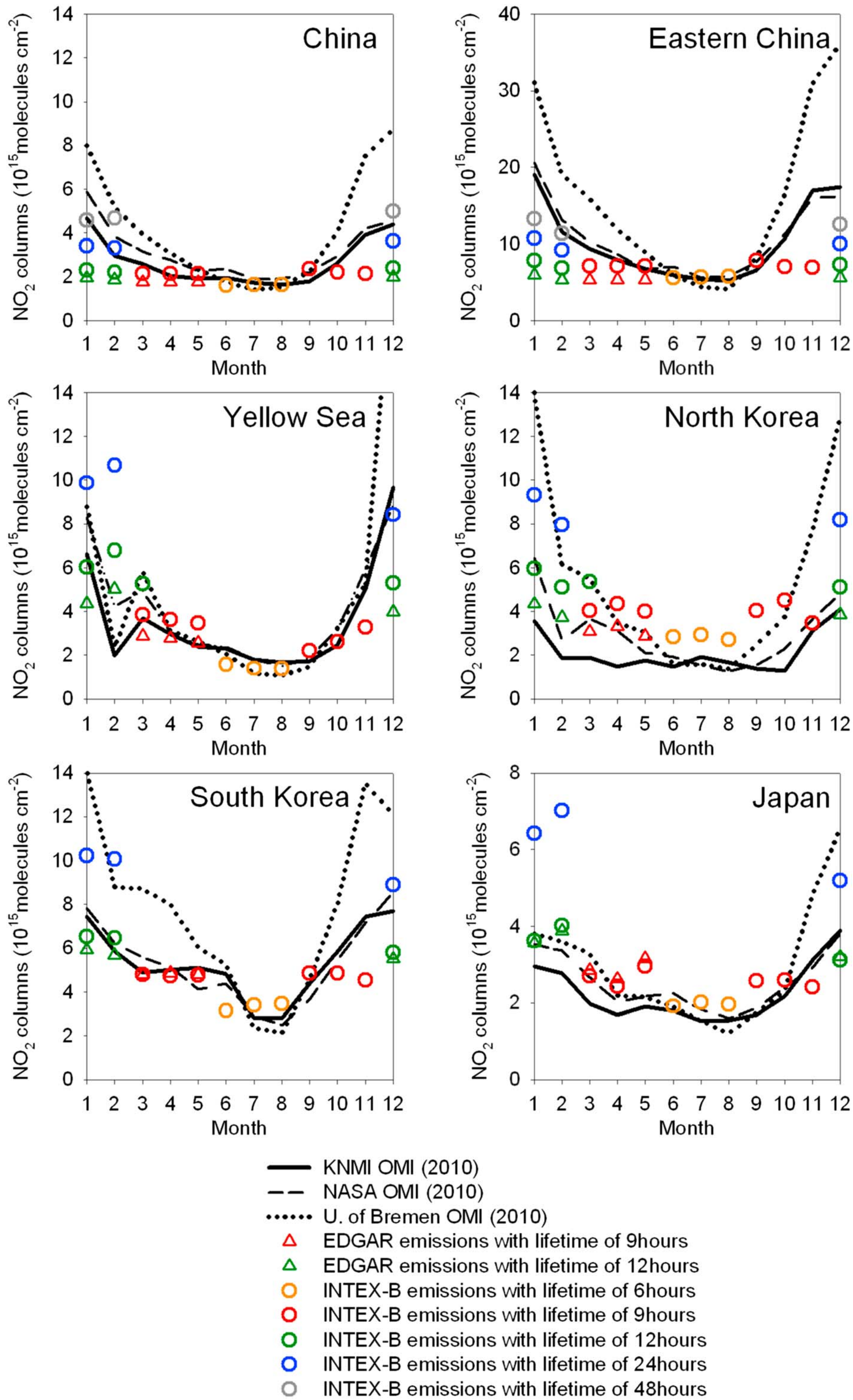

Figure 9. Monthly OMI NO_2 columns and FLEXPART NO_2 columns calculated using the INTEX-B (circles) and the EDGARv4.2 (triangles) inventories with various NO_x lifetimes. Grey, blue, green, red, and orange symbols represent FLEXPART results with NO_x lifetimes of 48, 24, 12, 9, and 6 h, respectively. The black lines represent the monthly OMI NO_2 columns from the KNMI (solid), NASA (dashed), and the University of Bremen (dotted) retrievals.

Table 3. The Same as Table 2 Except for NOx Lifetimes of 12, 9, 6, and 9 h for DJF, MAM, JJA, and SON, Respectively[a]

	Winter (DJF) - Lifetime: 12 h		
Receptor (Averaged Column Amount)	China (2.30)	Korea (5.83)	Japan (3.59)
Source			
China	98.43	67.19	34.55
Korea	1.33	32.07	13.81
Japan	0.24	0.74	51.64
	Spring (MAM) - Lifetime: 9 h		
Receptor (Averaged Column Amount)	China (2.15)	Korea (4.45)	Japan (2.69)
Source			
China	98.81	48.84	16.39
Korea	1.02	49.17	11.41
Japan	0.17	1.99	72.20
	Summer (JJA) - Lifetime: 6 h		
Receptor (Averaged Column Amount)	China (1.63)	Korea (3.08)	Japan (1.96)
Source			
China	99.40	30.32	1.75
Korea	0.60	68.36	4.24
Japan	0.00	1.32	94.01
	Autumn (SON) - Lifetime: 9 h		
Receptor (Averaged Column Amount)	China (2.24)	Korea (4.38)	Japan (2.52)
Source			
China	98.86	38.30	7.49
Korea	1.00	58.89	7.39
Japan	0.14	2.81	85.12

[a]Averaged column amount unit: 10^{15} molecules cm^{-2}. Areas of China (9,659,653 km^2), Korea (391,148 km^2), and Japan (784,219 km^2) were used to calculate averaged column amount, as shown in Figure 1.

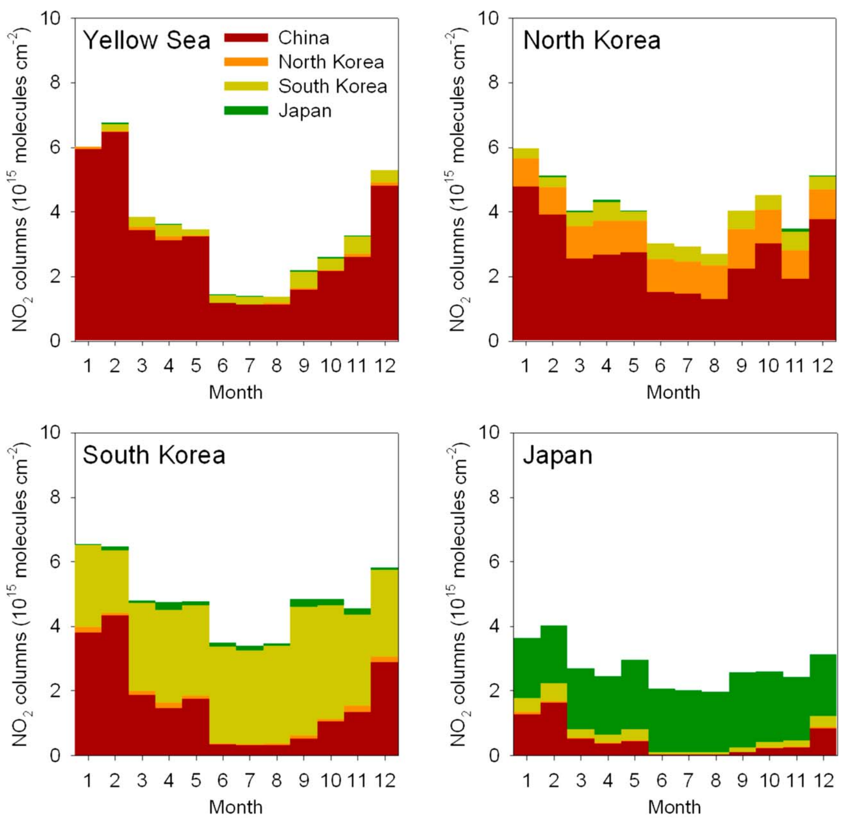

Figure 10. The same as Figure 8, except that the NO_x lifetimes in FLEXPART were set to 12, 9, 6 and 9 h in winter (DJF), spring (MAM), summer (JJA), and autumn (SON), respectively.

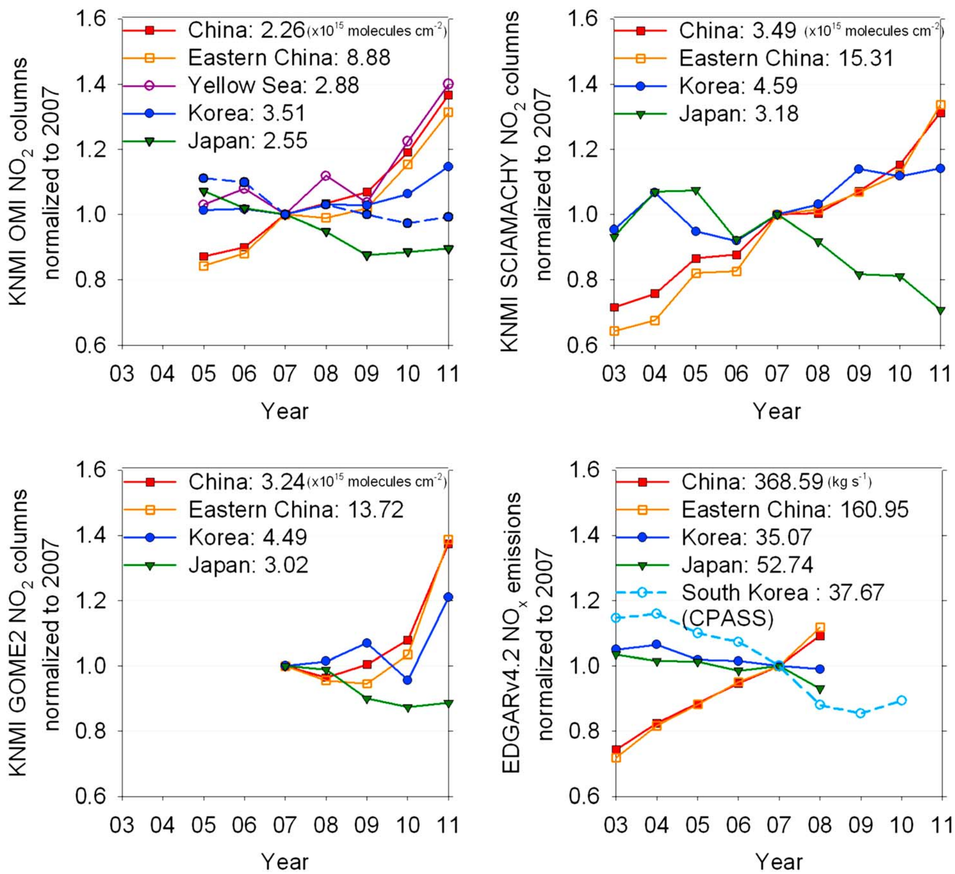

Figure 11. Interannual trends in satellite NO_2 columns and bottom-up NO_x emissions, normalized to the year 2005. Red-filled square, orange open square, purple open circle, blue-filled circle, and green triangle with solid lines denote trends in China, Eastern China, the Yellow Sea, Korea, and Japan, respectively. The blue dashed line with circles in the top left panel is the OMI NO_2 column trend in Korea after the impact of Chinese sources on Korea is removed. OMI, SCIAMACHY, GOME2, EDGARv4.2, and CAPSS09 data cover the periods 2005–2011, 2003–2011, 2007–2011, 2003–2008, and 2003–2010, respectively. 2007 values of NO_2 columns and NO_x emissions (kilograms of NO_2) used for normalization are listed in each panel.

with the constant NO_x lifetime simulations shown in Figure 8. The contribution of Chinese emissions to the total budget over all regions using a seasonally varying NO_x lifetime is smallest during summer, which is different from the results using a constant NO_x lifetime (Figure 8), in which the minimum influence of China occurs in autumn. The influence of Chinese sources on the Yellow Sea, South Korea, and Japan is the largest in the winter and the second largest in the spring, which may be linked to the secondary peaks of NO_2 seen in the satellite and surface observations in these regions. The impact of Chinese emissions on North Korea in autumn is equivalent to that in spring.

3.5. Implications of Trends in NO_x and O_3 in South Korea

While we used INTEX-B NO_x emissions for the year 2006 and EDGARv4.2 for the year 2005 in the 2010 FLEXPART model simulations, trend analysis of multisatellite data suggests NO_x emissions in China potentially increased by 40% between 2005 and 2010 (Figure 11). We infer that present-day contributions of NO_x emissions from China to other neighboring countries in East Asia are potentially greater than those demonstrated for 2010. Figure 11 shows that NO_2 columns from OMI [*Levelt et al.*, 2006], SCIAMACHY [*Bovensmann et al.*, 1999], and GOME2 [*Valks et al.*, 2011] consistently increased over China, Eastern China, and Korea but decreased over Japan in recent years. The NO_2 products of SCIAMACHY and GOME2 are derived with the same basic algorithm as OMI in section 2 (see *Boersma et al.* [2004] and *Boersma et al.* [2011] for details). NO_x emissions in EDGARV4.2 also indicate an increasing trend over China and a decreasing trend over Japan (Figure 11). However, the increasing satellite NO_2 column trend over Korea is not consistent with

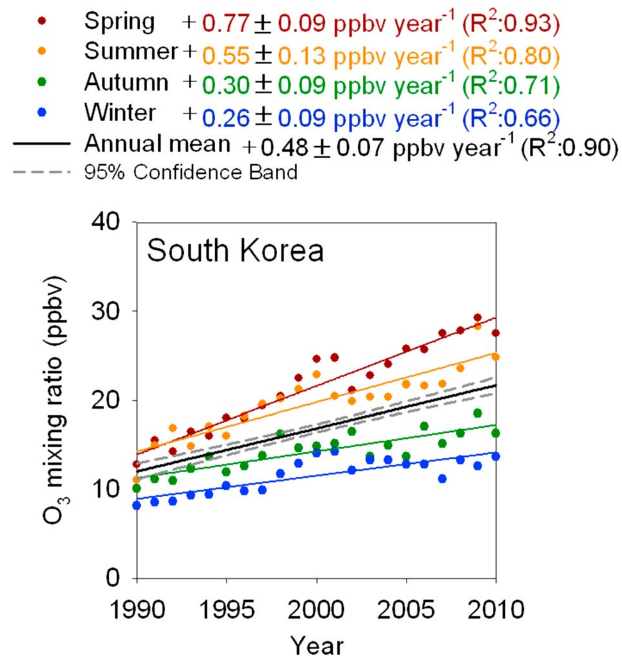

Figure 12. Trend in annual and seasonal average of hourly surface ozone in South Korea from 1990 to 2010, based on the monitoring data from the Korea Ministry of Environment. Red, orange, green, and blue circles denote ozone values in spring, summer, autumn, and winter, respectively. Trend lines from linear regression are also plotted. Black (solid) and gray (dashed) lines indicate annual average and 95% confidence limits, respectively. The rates of ozone increase (ppbv yr^{-1}) are shown above the plot with associated R^2 (coefficient of determination) values.

the slightly decreasing NO_x emissions trend in EDGARv4.2 and CAPSS09. The OMI data also show an increasing trend in NO_2 columns over the Yellow Sea, both in normalized and absolute values. When the impact of Chinese sources on Korea (ΔNO_2) is removed from the OMI trend (Figure 11, dashed blue line), assuming that ΔNO_2 in 2010 is ~46% of total NO_2 columns over Korea (Table 3) and in the other years ΔNO_2 is scaled from ΔNO_2 in 2010 by multiplying normalized NO_2 column trend over China to 2010 value, NO_2 columns over Korea show a negative trend, suggesting the importance of transport of NO_x in deriving the satellite-based trend in these areas. Because of interannual variability of satellite NO_2 columns above the Yellow Sea and Korea during this period, a longer satellite data record will be required to obtain reliable trends over these regions that can be used to understand the roles of emissions changes and transport.

Finally, the impact of springtime transport of NO_x on ozone in Korea is investigated. Figure 12 shows trends in surface ozone in South Korea in each season using all hourly measurements at 56 urban sites from 1990 to 2010. Ozone increased from 1990 to 2010 in all seasons, at a statistically significant rate $\geq$ 0.26 ppbv yr^{-1} and $R^2 \geq 0.66$. The springtime increase in ozone is the largest, with a rate of 0.77 ppbv yr^{-1} and $R^2 = 0.93$, similar to the springtime rate of increase at the baseline site of Mt. Happo in western Japan [*Parrish et al.*, 2012]. Ozone mixing ratios in spring and summer were quite similar in the 1990s, but springtime ozone levels have been larger than those in summer since the late 1990s, which is consistent with the large increase in Chinese emissions during this period [e.g., *Richter et al.*, 2005]. *Cooper et al.* [2010] reported a statistically significant increase in free tropospheric springtime ozone above western of North America and found that the trend was strongest when the sampled air masses were directly transported from South and East Asia.

Figures 13 and 14 show daytime and nighttime ozone trends, respectively, using data from multiple urban monitors in several regions scattered across South Korea. All the sites in Figure 13 have at least 20 years of data and demonstrate positive trends in daytime ozone during all seasons, with the rate of increase in spring greater than or equal to the rate in summer. At night, most of the sites show increasing ozone trends during all seasons (Figure 14). Note that the increase in nighttime ozone in spring is also larger than in summer, which may indicate the importance of the transport of ozone and precursors in springtime.

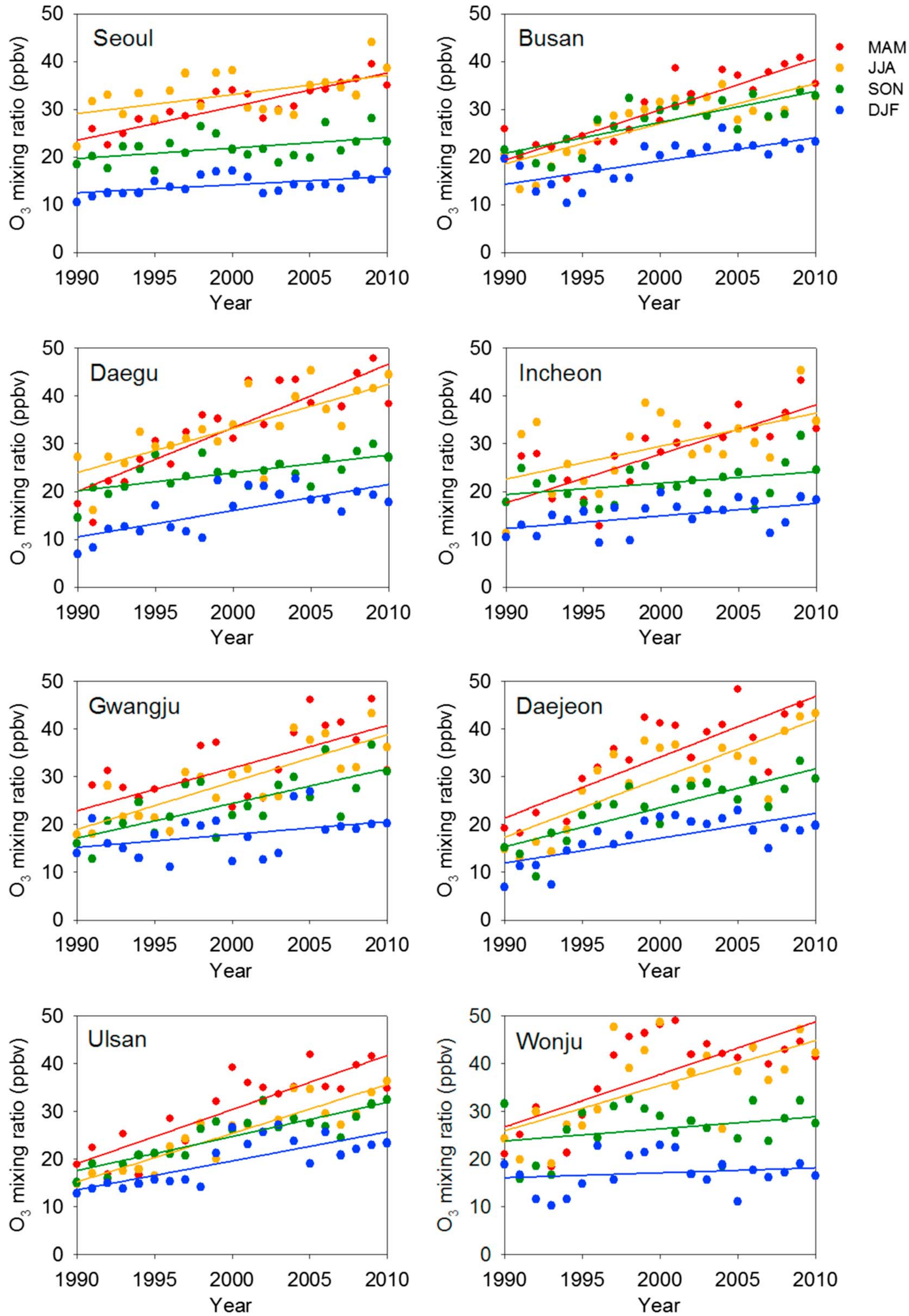

Figure 13. Year-to-year variations of hourly surface ozone averaged for each season from monitors in several urban areas in South Korea using only daytime measurements (1100–1700 LST).

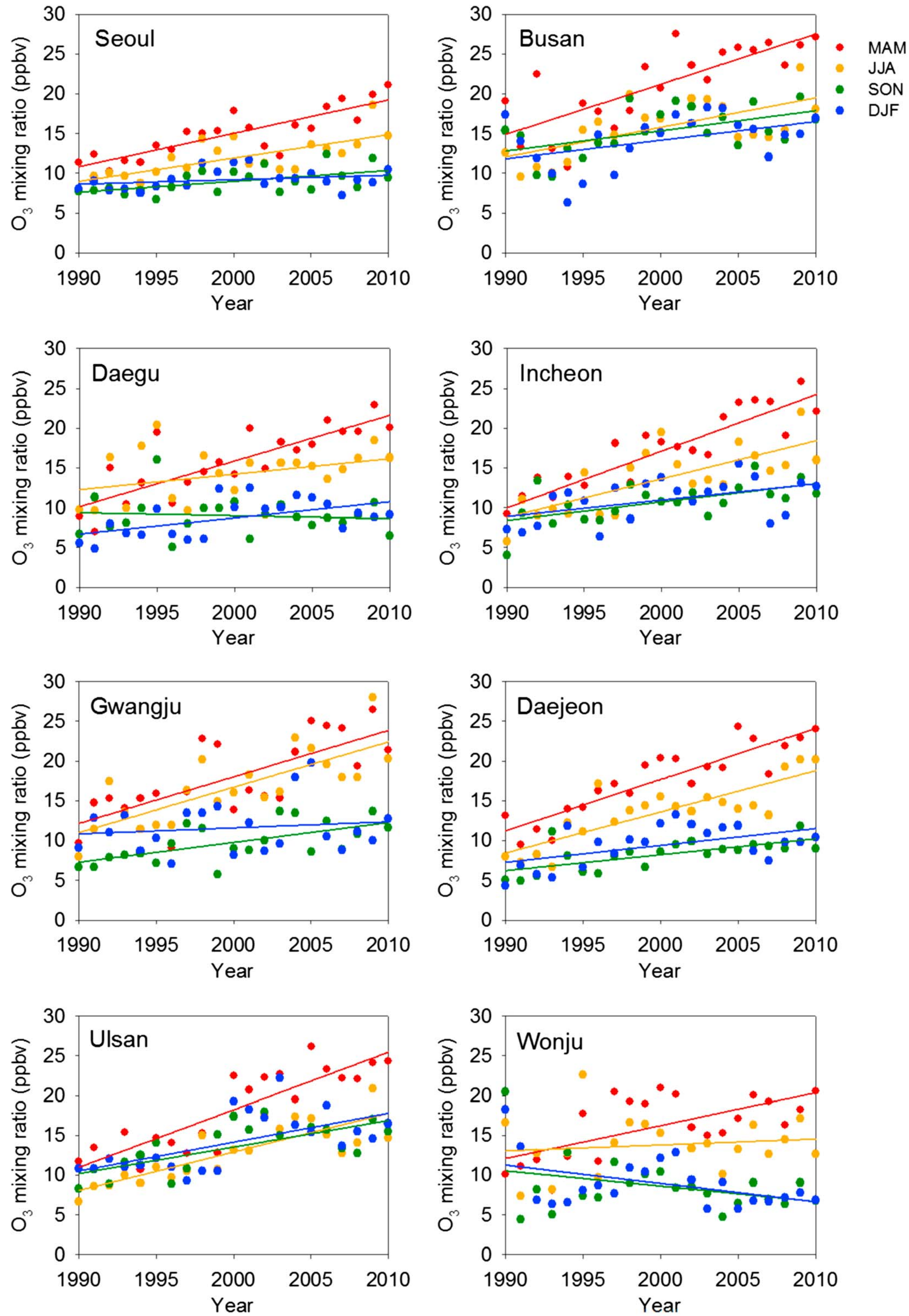

Figure 14. The same as Figure 13 but for nighttime (0000–0600LST).

Nighttime ozone in Wonju differs from that at the other Korean sites shown in Figures 14, with decreasing trends in autumn and winter. Wonju is located in mountainous terrain at an intersection of two major highways spanning South Korea. The east-west highway (Yeongdong Expressway) has been substantially augmented during 1990–2010. Causes for the decreasing nighttime ozone seen in Wonju need to be examined in context of local emissions changes, local circulation and the location of the monitor within complex terrain.

4. Conclusions

We investigated the spatial distributions of satellite tropospheric NO_2 columns and their seasonality in East Asia. NO_2 columns observed from space show high levels of NO_2 over low-emission areas, the Yellow Sea, and the East Sea. This finding indicates that NO_x originating from Korea and China can significantly impact the marine regions adjacent to these countries.

Unexpected seasonal variations of NO_2 columns were found downwind of China, including higher NO_2 columns in the spring over Korea, Japan, and the marine regions in between. These springtime peaks are also observed in NO_2 mixing ratios at surface sites in Korea and are further demonstrated in simulations of a Lagrangian particle dispersion model, but only if the NO_x lifetime is allowed to vary seasonally within the ranges indicated by atmospheric chemistry models. The springtime peaks in NO_2 abundance over these downwind regions of East Asia are consistent with transport from China via fast, eastward moving synoptic disturbances that occur frequently during the spring.

This study illustrates that NO_x transport and emissions are both important for understanding the local budgets of NO_x across East Asia. For example, satellite tropospheric NO_2 columns show increasing trends over Korea since 2005, while Korean NO_x emissions from both global and national inventories show a slightly decreasing trend for the same period. The transport of NO_x emitted from Chinese sources to Korea can explain the discrepancies between the trends in the satellite observations and the emission inventories in Korea. This study suggests that NO_x transport should be considered in studies using satellite NO_2 retrievals to derive NO_x emissions at local scales particularly in regions adjacent to large emission sources, such as in East Asia, Europe, and the Eastern U.S.

Our study also found large uncertainties in satellite retrievals from different institutions, which consequently impact the estimation of NO_x lifetimes and the evaluation of bottom-up inventories using satellite data. The use of suborbital measurements of columns or vertical profiles of NO_2 and aerosols to calibrate the satellite retrievals could lead to a better understanding of uncertainties in space-based measurements and emission inventories for East Asia.

To examine the quantitative impact of each source on each receptor throughout the year, the monthly changes in the chemical lifetime of NO_x and its emissions should be examined using three-dimensional regional chemical-transport model simulations. Furthermore, relationship between atmospheric NO_2 columns and surface NOx emissions may not be linear and can be influenced by chemistry depending on atmospheric abundance of NO_x and volatile organic compounds. Using a three-dimensional chemical transport model will help to incorporate non-linear relationship between the NO_2 columns and the NO_x emissions. Examining the impact of springtime NO_x transport on ozone levels and trends in East Asia will be especially important, because South Korea's surface ozone has experienced its strongest growth in spring. Future studies should also consider the transport and chemistry of NO_x beyond East Asia across the North Pacific Ocean, using satellite observations, Lagrangian particle dispersion modeling, and three-dimensional chemical transport modeling.

Acknowledgments
The authors thank the European Commission, Joint Research Centre (JRC)/Netherlands Environmental Assessment Agency (PBL) for the Emission Database for Global Atmospheric Research (EDGAR), release version 4.2. http://edgar.jrc.ec.europa.eu, 2011. The Dutch-Finnish-built OMI is part of the NASA EOS Aura satellite payload. The OMI project is managed by NIVR and KNMI in the Netherlands. The authors acknowledge the free use of tropospheric NO_2 column data from the OMI, SCIAMACHY and GOME2 sensors from www.temis.nl and OMI data from NASA and University of Bremen. The NO_2 data products of GOME2 were generated using level 1 data developed within the O3MSAF project of the EUMETSAT. The Korea Meteorological Administration and Korea Ministry of Environment operate surface meteorological stations and air quality monitoring stations, respectively, in South Korea. This research was supported by Basic Science Research Program through the National Research Foundation of Korea (NRF) funded by the Ministry of Education (2013R1A1A2057732). The first author acknowledges support from the NOAA visiting scientist program. Rokjin Park was supported by the GEMS Program of the Ministry of Environment, Korea, and the Eco Innovation Program of KEITI (ARQ201204015). The NOAA Health of Atmosphere program also supported this study.

References

Acarreta, J. R., J. F. De Haan, and P. Stamnes (2004), Cloud pressure retrieval using the O_2-O_2 absorption band at 477 nm, *J. Geophys. Res.*, *109*, D05204, doi:10.1029/2003JD003915.

Boersma, K. F., H. J. Eskes and E. J. Brinksma (2004), Error analysis for tropospheric NO_2 retrieval from space, *J. Geophys. Res. 109*, D04311, doi:10.1029/2003JD003962.

Boersma, K. F., et al. (2007), Near-real time retrieval of tropospheric NO_2 from OMI, *Atmos. Chem. Phys.*, *7*, 2103–2118, doi:10.5194/acp-7-2103-2007.

Boersma, K. F., et al. (2011), An improved tropospheric NO_2 column retrieval algorithm for the Ozone Monitoring Instrument , *Atmos. Meas. Tech.*, *4*, 1905–1928.

Bovensmann, H., J. P. Burrows, M. Buchwitz, J. Frerick, S. Noel, V. V. Rozanov, K. V. Chance, and A. P. H. Goede (1999), SCIAMACHY: Mission objectives and measurement modes, *J. Atmos. Sci.*, *56*(2), 127–150.

Brioude, J., O. R. Cooper, G. Feingold, M. Trainer, S. R. Freitas, D. Kowal, J. K. Ayers, S. A. McKeen, G. J. Frost and E.-Y. Hsie (2009), Effect of biomass burning on marine stratocumulus cloud off the California coast, *Atmos. Chem. Phys.*, *9*, 8841–8856.

Bucsela, E. J., N. A. Krotkov, E. A. Celarier, L. N. Lamsal, W. H. Swartz, P. K. Bhartia, K. F. Boersma, J. P. Veefkind, J. F. Gleason, and K. E. Pickering (2013), A new stratospheric and tropospheric NO_2 retrieval algorithm for nadir-viewing satellite instruments: Applications to OMI, *Atmos. Meas. Tech.*, *6*, 2607–2626.

Burrows, J. P., et al. (1999), The global ozone monitoring experiment (GOME): Mission concept and first scientific results, *J. Atmos. Sci.*, *56*(2), 151–175.

Calvert, J. G., A. Lazrus, G. L. Kok, B. G. Heikes, J. G. Walega, J. Lind, and C. A. Cantrell (1985), Chemical mechanisms of acid generation in the troposphere, *Nature*, *317*, 27–35.

Carmichael, G. R., et al. (2002), The MICS-Asia study: Model intercomparison of long-range transport and sulfur deposition in East Asia, *Atmos. Environ.*, *36*, 175–199.

Cooper, O. R., et al. (2010), Increasing springtime ozone mixing ratios in the free troposphere over western North America, *Nature*, *463*, 344–348, doi:10.1038/nature08708.

Dentener, F., M. van Weele, M. Krol, S. Houweling, and P. van Velthoven (2003), Trend and inter-annual variability of methane emissions derived from 1979-1993 global CTM simulations, *Atmos. Chem. Phys.*, *3*, 73–88.

Dirksen, R. J., K. F. Boersma, H. J. Eskes, D. V. Ionov, E. J. Bucsela, P. F. Levelt, and H. M. Kelder (2011), Evaluation of stratospheric NO_2 retrieved from the Ozone Monitoring Instrument: Intercomparison, diurnal cycle, and trending, *J. Geophys. Res.*, *116*, D08305, doi:10.1029/2010JD014943.

Duncan, B. N., et al. (2010), Application of OMI observations to a space-based indicator of NO_x and VOC controls on surface ozone formation, *Atmos. Environ.*, *44*, 2213–2223.

Dunlea, E. J., et al. (2007), Evaluation of nitrogen dioxide chemiluminescence monitors in a polluted urban environment, *Atmos. Chem. Phys.*, *7*, 2691–2704.

Eskes, H. J., and K. F. Boersma (2003), Averaging kernels for DOAS total-column satellite retrievals, *Atmos. Chem. Phys.*, *3*, 1285–1291.

Fehsenfeld, F. C., et al. (1987), A ground-based intercomparison of NO, NO_X, and NO_Y measurement techniques, *J. Geophys. Res.*, *92*(D12), 14,710–14,722.

Granier, C., and G. Brasseur (2003), The impact of road traffic on global tropospheric ozone, *Geophys. Res. Lett.*, *30*(2), 1086, doi:10.1029/2002GL015972.

Hilboll, A., A. Richter, and J. P. Burrows (2013), Long-term changes of tropospheric NO_2 over megacities derived from multiple satellite instruments, *Atmos. Chem. Phys.*, *13*, 4145–4169, doi:10.5194/acp-13-4145-2013.

Jaeglé, L., D. J. Jacob, Y. Wang, A. J. Weinheimer, B. A. Ridley, T. L. Campos, G. W. Sachse, and D. E. Hagen (1998), Sources and chemistry of NO_x in the upper troposphere over the United States, *Geophys. Res. Lett.*, *25*(10), 1705–1708.

Jaeglé, L., R. V. Martin, K. Chance, L. Steinberger, T. P. Kurosu, D. J. Jacob, A. I. Modi, V. Yoboue, L. Sigha-Nkamdjou, and C. Galy-Lacaux (2004), Satellite mapping of rain-induced nitric oxide emissions form soil, *J. Geophys. Res.*, *109*, D21310, doi:10.1029/2004JD004787.

Jeong, G.-R., and I. N. Sokolik (2007), Effect of mineral dust aerosols on the photolysis rates in the clean and polluted marine environments, *J. Geophys. Res.*, *112*, D21308, doi:10.1029/2007JD008442.

Kim, S.-W., S.-U. Park, and B. Lee (1997), Variations of SO_2, NO_X, CO and O_3 concentrations in association with synoptic meteorological conditions, *J. Korean Meteorol. Soc.*, *33*, 2, 273–287.

Kim, S.-W., A. Heckel, S. A. McKeen, G. J. Frost, E.-Y. Hsie, M. K. Trainer, A. Richter, J. P. Burrows, S. E. Peckham, and G. A. Grell (2006), Satellite-observed U.S. power plant NO_x emission reductions and their impact on air quality, *Geophys. Res. Lett.*, *33*, L22812, doi:10.1029/2006GL027749.

Kim, S.-W., A. Heckel, G. J. Frost, A. Richter, J. Gleason, J. P. Burrows, S. McKeen, E.-Y. Hsie, C. Granier, and M. Trainer (2009), NO_2 columns in the western United States observed from space and simulated by a regional chemistry model and their implications for NO_x emissions, *J. Geophys. Res.*, *114*, D11301, doi:10.1029/2008JD011343.

Kim, S.-W., et al. (2011), Evaluations of NO_x and highly reactive VOC emission inventories in Texas and their implications for ozone plume simulations during the Texas Air Quality Study 2006, *Atmos. Chem. Phys.*, *11*, 11,361–11,386, doi:10.5194/acp-11-11361-2011.

Kleipool, Q. L., M. R. Dobber, J. F. de Haan, and P. F. Levelt (2008), Earth surface reflectance climatology from 3 years of OMI data, *J. Geophys. Res.*, *113*, D18308, doi:10.1029/2008JD010290.

Lamarque, J.-F., J. T. Kiehl, P. G. Hess, W. D. Collins, L. K. Emmons, P. Ginoux, C. Luo, and X. X. Tie (2005), Response of a coupled chemistry-climate model to changes in aerosol emissions: Global impact on the hydrological cycle and the tropospheric burdens of OH, ozone, and NO_x, *Geophys. Res. Lett.*, *32*, L16809, doi:10.1029/2005GL023419.

Lamsal, L. N., R. V. Martin, A. van Donkelaar, E. A. Celarier, E. J. Bucsela, K. F. Boersma, R. Dirksen, C. Luo, and Y. Wang (2010), Indirect validation of tropospheric nitrogen dioxide retrieved from the OMI satellite instrument: Insight into the seasonal variation of nitrogen oxides at northern midlatitudes, *J. Geophys. Res.*, *115*, D05302, doi:10.1029/2009JD013351.

Lamsal, L. N., R. V. Martin, A. Padmanabhan, A. van Donkelaar, Q. Zhang, C. E. Sioris, K. Chance, T. P. Kurosu, and M. J. Newchurch (2011), Application of satellite observations for timely updates to global anthropogenic NO_x emission inventories, *Geophys. Res. Lett.*, *38*, L05810, doi:10.1029/2010GL046476.

Lawrence, M. G., and P. J. Crutzen (1999). Influence of NO_x emissions from ships on tropospheric photochemistry and climate, *Nature*, *402*, 167–170.

Leue, C., M. Wenig, T. Wagner, O. Klimm, U. Platt, and B. Jahne (2001), Quantitative analysis of NO_x emissions from GOME satellite image sequences, *J. Geophys. Res.*, *106*(D6), 5493–5505.

Levelt, P. F., G. H. J. van den Oord, M. R. Dobber, A. Mälkki, H. Visser, J. de Vries, P. Stammes, J. Lundell, and H. Saari (2006), The Ozone Monitoring Instrument, *IEEE Trans. Geosci. Remote Sens.*, *44*(5), 1093–1101, doi:10.1109/TGRS.2006.872333.

Liang, Q., L. Jaeglé, D. A. Jaffe, P. Weiss-Penzias, A. Heckman, and J. A. Snow (2004), Long-range transport of Asian pollution to the northeast Pacific: Seasonal variations and transport pathways of carbon monoxide, *J. Geophys. Res.*, *109*, D23S07, doi:10.1029/2003JD004402.

Lin, C.-Y., S. C., Liu, C. C.-K. Chou, S.-J., Huang, C.-M. Liu, C. H. Kuo, and C.-Y. Young (2005), Long-range transport of aerosols and their impact on the air quality of Taiwan, *Atmos. Environ.*, *39*, 6066–6076.

Lin, J.-T. (2012), Satellite constraint for emissions of nitrogen oxides from anthropogenic, lightning and soil sources over East China on a high-resolution grid, *Atmos. Chem. Phys.*, *12*, 2881–2898, doi:10.5194/acp-12-2881-2012.

Lin, M., T. Holloway, G. R. Carmichael, and A. M. Fiore (2010), Quantifying pollution inflow and outflow over East Asia in spring with regional and global models, *Atmos. Chem. Phys.*, *10*, 4221–4239.

Lin, M., et al. (2012), Transport of Asian ozone pollution into surface air over the western United States in spring, *J. Geophys. Res.*, *117*, D00V07, doi:10.1029/2011JD016961.

Liu, H., D. J. Jacob, I. Bey, R. M. Yantosca, B. N. Duncan, and G. W. Sachse (2003), Transport pathways for Asian pollution outflow over the Pacific: Interannual and seasonal variations, *J. Geophys. Res.*, *108*(D20), 8786, doi:10.1029/2002JD003102.

Martin, R. V., D. J. Jacob, K. Chance, T. P. Kurosu, P. I. Palmer, and M. J. Evans (2003a), Global inventory of nitrogen oxides emissions constrained by space-based observations of NO_2 columns, *J. Geophys. Res.*, *108*(D17), 4537, doi:10.1029/2003JD003453.

Martin, R. V., D. J. Jacob, R. M. Yantosca, M. Chin, and P. Ginoux (2003b), Global and regional decreases in tropospheric oxidants from photochemical effects of aerosols, *J. Geophys. Res.*, *108*(D3), 4097, doi:10.1029/2002JD002622.

Park, R. J., D. J. Jacob, B. D. Field, R. M. Yantosca and M. Chin (2004), Natural and transboundary pollution influences on sulfate-nitrate-ammonium aerosols in the United States: Implications for policy. *J. Geophys. Res. 109*, D15204, doi:10.1029/2003JD004473.

Park, I.-S., W.-J. Choi, T.-Y. Lee, S.-J. Lee, J.-S. Han, and C.-H. Kim (2005), Simulation of long-range transport of air pollutants over Northeast Asia using a comprehensive acid deposition model, *Atmos. Environ.*, *39*, 4075–4085.

Parrish, D. D., et al. (2012), Long-term changes in lower tropospheric baseline ozone concentrations at northern mid-latitudes, *Atmos. Chem. Phys.*, *12*, 11,485–11,504, doi:10.5194/acp-12-11485-2012.

Platt, U., and J. Stutz (2008), *Differential Optical Absorption Spectroscopy: Principles and Applications*, 597 pp., Springer Verlag, Heidelberg, ISBN:978-3540211938.

Richter, A., J. P. Burrows, H. Nub, C. Granier, and U. Niemeier (2005), Increase in tropospheric nitrogen dioxide levels over China observed from space, *Nature*, *437*, 129–132.

Russell, A. R., L. C. Valin, and R. C. Cohen (2012), Trends in OMI NO_2 observations over the US: Effects of emission control technology and the economic recession, *Atmos. Chem. Phys. Discuss.*, *12*, 15,419–15,452, doi:10.5194/acpd-12-15419-2012.

Stammes, P. (2001), Spectral radiance modelling in the UV-Visible range, in *IRS 2000: Current Problems in Atmospheric Radiation*, edited by W. L. Smith and Y. M. Timofeyev, pp. 385–388, A. Deepak Publ., Hampton (VA).

Stavrakou, T., J.-F. Muller, K. F. Boersma, I. De Smedt, and R. J. van der A (2008), Assessing the distribution and growth rates of NO_x emission sources by inverting a 10-year record of NO_2 satellite columns, *Geophys. Res. Lett.*, *35*, L10801, doi:10.1029/2008GL033521.

Stohl, A., S. Eckhardt, C. Forster, P. James, and N. Spichtinger (2002), On the pathways and timescales of intercontinental air pollution transport, *J. Geophys. Res.*, *107*(D23), 4684, doi:10.1029/2001JD001396.

Stohl, A., C. Forster, A. Frank, P. Seibert, and G. Wotawa (2005), Technical note: The Lagrangian particle dispersion model FLEXPART version 6.2. *Atmos. Chem. Phys. Discuss.*, *5*, 4739–4799.

Stohl, A., et al. (2007), Arctic smoke-record high air pollution levels in the European Arctic due to agricultural fires in Eastern Europe in spring 2006, *Atmos. Chem. Phys.*, *7*, 511–534.

Stohl, A., et al. (2011), Determination of time-and height-resolved volcanic ash emissions and their use for quantitative ash dispersion modeling: The 2010 Eyjafjallajökull eruption, *Atmos. Chem. Phys.*, *11*, 4333–4351.

Uno, I., K. Eguchi, K. Yuminoto, T. Takemura, A. Shimizu, M. Uematsu, Z. Liu, Z. Wang, Y. Hara, and N. Sugimoto (2009), Asian dust transported one full circuit around the globe, *Nat. Geosci.*, *2*, 557–560, doi:10.1038/ngeo583.

Valks, P., G. Pinardi, A. Richter, J.-C. Lambert, N. Hao, D. Loyola, M. Van Roozendael, and S. Emmadi (2011), Operational total and tropospheric NO_2 column retrieval from GOME-2, *Atmos. Meas. Tech.*, *4*, 1491–1514, doi:10.5194/amt-4-1491-2011.

van der A, R. J., D. H. M. U. Peters, H. Eskes, K. F. Boersma, M. Van Roozendael, I. De Smedt, and H. M. Kelder (2006), Detection of the trend and seasonal variation in tropospheric NO_2 over China, *J. Geophys. Res.*, *111*, D12317, doi:10.1029/2005JD006594.

van der A, R. J., H. J. Eskes, K. F. Boersma, T. P. C. van Noije, M. Van Roozendael, I. De Smedt, D. H. M. U. Peters, and E. W. Meijer (2008), Trends, seasonal variability and dominant NO_x source derived from a ten year record of NO_2 measured from space, *J. Geophys. Res.*, *113*, D04302, doi:10.1029/2007JD009021.

Wang, S. W., Q. Zhang, D. G. Streets, K. B. He, R. V. Martin, L. N. Lamsal, D. Chen, Y. Lei, and Z. Lu (2012), Growth in NO_x emissions from power plants in China: Bottom-up estimates and satellite observations, *Atmos. Chem. Phys.*, *12*, 4429–4447, doi:10.5194/acp-12-4429-2012.

Warneke, C., et al. (2009), Biomass burning in Siberia and Kazakhstan as an important source for haze over the Alaskan Arctic in April 2008, *Geophys. Res. Lett.*, *36*, L02813, doi:10.1029/2008GL036194.

Wenig, M., N. Spichtinger, A. Stohl, G. Held, S. Beirle, T. Wanger, B. Jahne, and U. Platt (2003), Intercontinental transport of nitrogen oxide pollution plumes, *Atmos. Chem. Phys.*, *3*, 387–393.

Wild, O., M. J. Prather, and H. Akimoto (2001), Indirect long-term global radiative cooling from NO_x emissions, *Geophys. Res. Lett.*, *28*(9), 1719–1722.

Zhang, Q., et al. (2007), NO_x emission trends for China, 1995-2004: The view from the ground and the view from space, *J. Geophys. Res.*, *112*, D22306, doi:10.1029/2007JD008684.

Zhang, L., et al. (2008), Transpacific transport of ozone pollution and the effect of recent Asian emission increases on air quality in North America: An integrated analysis using satellite, aircraft, ozonesonde, and surface observations, *Atmos. Chem. Phys.*, *8*, 6117–6136.

Zhang, Q., et al. (2009), Asian emissions in 2006 for the NASA INTEX-B mission, *Atmos. Chem. Phys.*, *9*, 5131–5153, doi:10.5194/acp-9-5131-2009.